cmgh
CELLULAR AND MOLECULAR GASTROENTEROLOGY AND HEPATOLOGY

ORIGINAL RESEARCH

Prolonged Absence of Mechanoluminal Stimulation in Human Intestine Alters the Transcriptome and Intestinal Stem Cell Niche

Minna M. Wieck,[1,2,*] Christopher R. Schlieve,[1,2,*] Matthew E. Thornton,[3] Kathryn L. Fowler,[1] Mubina Isani,[1,2] Christa N. Grant,[1,2] Ashley E. Hilton,[4] Xiaogang Hou,[1] Brendan H. Grubbs,[3] Mark R. Frey,[1,5] and Tracy C. Grikscheit[1,2,4]

[1]*Developmental Biology and Regenerative Medicine Program, Saban Research Institute,* [2]*Department of Pediatric Surgery, Children's Hospital Los Angeles, Los Angeles, California;* [3]*Department of Obstetrics and Gynecology,* [5]*Department of Pediatrics and Biochemistry, Department of Molecular Biology,* [4]*Keck School of Medicine, University of Southern California, Los Angeles, California*

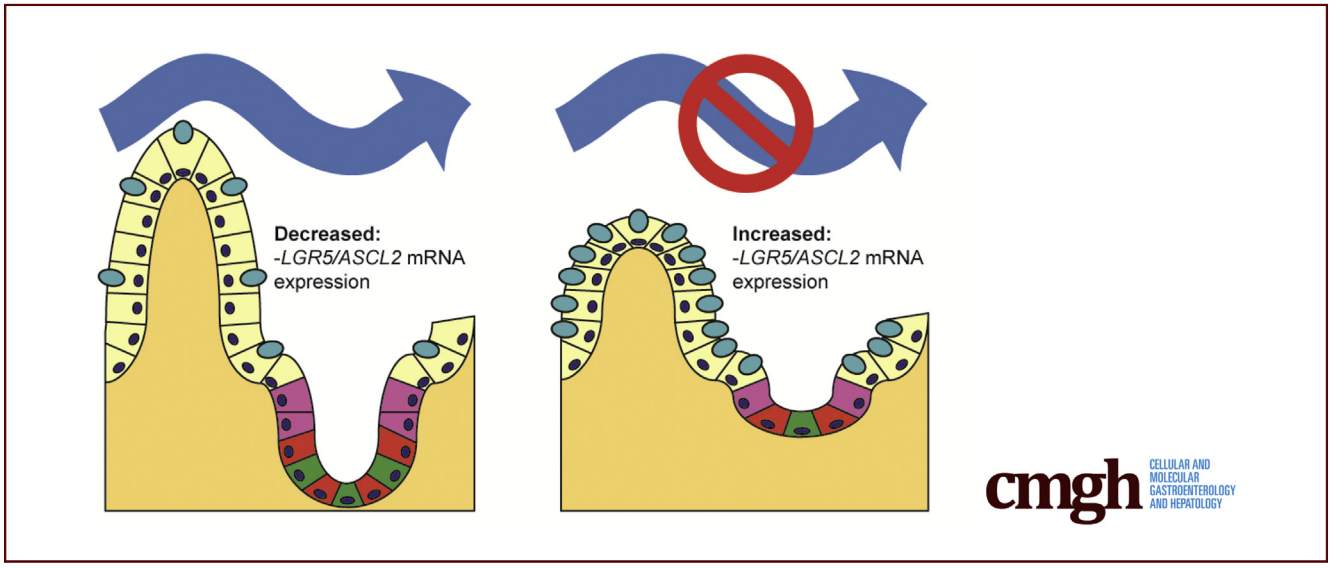

SUMMARY

The absence of intestinal mechanoluminal stimulation in calorically replete patients decreases proliferation, villus height, crypt depth, and the intestinal stem cell population. Altered genes involved in proliferation, digestion, and inflammation may be targets for enhancing adaptation in short-bowel syndrome patients.

BACKGROUND & AIMS: For patients with short-bowel syndrome, intestinal adaptation is required to achieve enteral independence. Although adaptation has been studied extensively in animal models, little is known about this process in human intestine. We hypothesized that analysis of matched specimens with and without luminal flow could identify new potential therapeutic pathways.

METHODS: Fifteen paired human ileum samples were collected from children aged 2–20 months during ileostomy-reversal surgery after short-segment intestinal resection and diversion. The segment exposed to enteral feeding was denoted as fed, and the diverted segment was labeled as unfed. Morphometrics and cell differentiation were compared histologically. RNA Sequencing and Gene Ontology Enrichment Analysis identified over-represented and under-represented pathways. Immunofluorescence staining and Western blot evaluated proteins of interest. Paired data were compared with 1-tailed Wilcoxon rank-sum tests with a P value less than .05 considered significant.

RESULTS: Unfed ileum contained shorter villi, shallower crypts, and fewer Paneth cells. Genes up-regulated by the absence of mechanoluminal stimulation were involved in digestion, metabolism, and transport. Messenger RNA expression of *LGR5* was significantly higher in unfed intestine, accompanied by increased levels of phosphorylated signal transducer and activator of transcription 3 protein, and *CCND1* and C-*MYC* messenger RNA. However, decreased proliferation and fewer LGR5+, OLFM4+, and SOX9+ intestinal stem cells (ISCs) were observed in unfed ileum.

CONCLUSIONS: Even with sufficient systemic caloric intake, human ileum responds to the chronic absence of mechanoluminal stimulation by up-regulating brush-border enzymes, transporters, structural genes, and ISC genes *LGR5* and *ASCL2*. These data suggest that unfed intestine is primed to replenish the ISC population upon re-introduction of enteral

feeding. Therefore, the elucidation of pathways involved in these processes may provide therapeutic targets for patients with intestinal failure. RNA sequencing data are available at Gene Expression Omnibus series GSE82147. *(Cell Mol Gastroenterol Hepatol 2017;3:367–388; http://dx.doi.org/10.1016/j.jcmgh.2016.12.008)*

Keywords: Intestinal Stem Cell; LGR5; Small Intestine; Calorie Restriction; Enteric Nutrition; Mechanoluminal Flow.

See editorial on page 297.

Short-bowel syndrome (SBS) is a highly morbid and costly disease resulting from insufficient intestinal length or inadequate intestinal absorption. In children, SBS may develop after massive small-bowel resection for a range of diseases including necrotizing enterocolitis (NEC), intestinal atresia, and volvulus. Enteral independence from supplemental parental nutrition relies on adaptation of the remaining bowel. In animal models, adaptation is characterized by taller villi, deeper crypts, increased bowel diameter and length, and increased proliferation and apoptosis in the remaining bowel.[1–5] However, these changes have been inconsistently found in human intestine after resection.[6–9] Further investigation is necessary to understand regulatory mechanisms that direct adaptation in human intestine.

Several growth factors and hormones have been identified that may enhance adaptation, most notably growth hormone and glucagon-like peptide 2.[10–13] However, there are many more regulators of intestinal epithelial proliferation, such as immune and inflammatory systems, microbial components, and mechanoluminal stimulation.[14] The mechanisms mediating these effects are incompletely understood.[15,16] Knowledge of how these diverse mitogens affect proliferation and intestinal stem cell (ISC) activity might help to identify novel therapeutic pathways and agents for SBS.

Prompt and nutritionally appropriate initiation of enteral feeds is a critical component of intestinal rehabilitation programs and is associated with shorter hospitalizations, shorter duration of parenteral nutrition, and increased rates of enteral autonomy.[17–19] Enteral nutrition may enhance intestinal adaptation via induction of various gastrointestinal hormones and pancreaticobiliary secretions or direct stimulation of intestinal epithelium, but the exact effects induced by mechanoluminal stimulation are unknown.

Animal studies of enteral nutrition often are confounded by differences in caloric status and types of nutrition.[20–22] In human beings, comorbidities associated with the underlying pathology requiring intestinal resection also must be considered. Thus, we sought to determine the isolated effects of mechanoluminal stimulation on human intestine, independent of such confounders, by comparing closely paired proximal and distal limbs from ileostomy resections in infants with previous NEC or focal intestinal perforation (Figure 1*A*). To exclude differences caused by regional anatomic variances, we only included matched samples with a minimum of intervening intestinal resection. This allowed us to test a hypothesis that in matched human samples, mechanoluminal flow is a potent mitogen with multiple in vivo effects on cellular differentiation and genetic programming. We found that withdrawing luminal flow decreased common measures of adaptation, including villus height, crypt depth, proliferation, and various ISC populations. In addition, we recognized that in the distal limb of intestine diverted from enteric feeding, up-regulated genes were associated with digestion and metabolism while down-regulated genes were associated with cell proliferation and inflammation. This approach also identified candidate mediators of proliferation that may lead to novel therapeutic targets for enhancing intestinal adaptation.

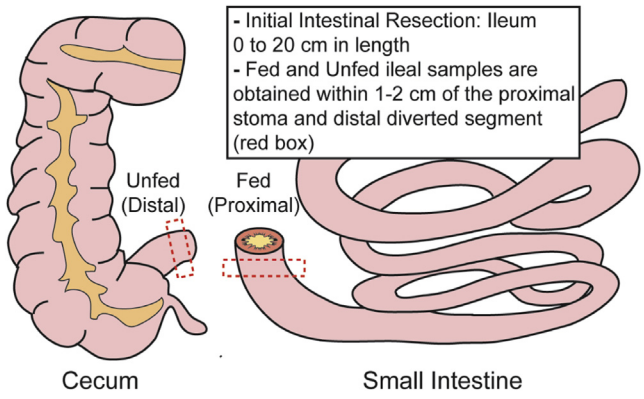

Figure 1. (*A*) Schematic illustration depicting intestinal diversion in our patient group. The proximal fed portion of the small intestine receives mechanoluminal stimulation through enteric feeding. The distal unfed portion of diverted small intestine does not see mechanoluminal stimulation for a minimum period of 7 weeks. The length of intestinal resection ranged from 0 to 20 cm in length, with an average resection of 5 cm. Upon ileostomy takedown and anastomosis, samples procured for the study were obtained within 1–2 cm proximal to the stoma in fed intestine and 1–2 cm distal to the diverted unfed pouch (*red dotted boxes*).

Materials and Methods

The research protocol was approved by the Children's Hospital Los Angeles institutional review board (CCI-09-00093). All authors had access to the study data and reviewed and approved the final manuscript.

Patient Population

All patients undergoing small intestinal anastomosis after ileostomy at our institution between August 2012 and

*Authors share co-first authorship.

Abbreviations used in this paper: **ISC, intestinal stem cell; mRNA, messenger RNA; NEC, necrotizing enterocolitis; PCR, polymerase chain reaction; qPCR, quantitative polymerase chain reaction; SBS, short-bowel syndrome; STAT3, signal transducer and activator of transcription 3; Wnt, wingless-related integration site.**

Most current article

2352-345X
http://dx.doi.org/10.1016/j.jcmgh.2016.12.008

October 2016 were identified by review of surgical records. Inclusion criteria consisted of age younger than 2 years and previous diagnosis of NEC or focal intestinal perforation resulting in ileal resection. The diagnosis was based on clinical presentation, surgical findings, and final pathologic examination of the resected specimen. To minimize any discrepancies resulting from baseline variation in different intestinal segments, patients with long-segment bowel resection resulting in SBS were excluded. Charts were reviewed for demographic and treatment details, including location and amount of intestine resected, duration of intestinal diversion, timing of enteral and parenteral nutrition, ostomy complications, and postreversal complications.

Demographic and clinical characteristics of the 15 included patients are presented in Table 1. Medical chart review showed that 14 patients were premature infants who underwent resection before 5 weeks of age for focal intestinal perforation or NEC. After initial resection, all patients received broad-spectrum antibiotics for at least 10 days. All patients also received total parenteral nutrition and some enteral feeds either orally or via a feeding tube to achieve caloric repletion and appropriate weight gain. Only 5 infants were able to achieve complete enteral independence by the time of ileostomy reversal. Patients were diverted for 7–48 weeks, and afterward most still required total parenteral nutrition until they achieved enteral independence before discharge from the hospital. Ostomy complications occurred infrequently in our patient population. Peristomal hernias without obstruction occurred in 2 patients, and 1 patient underwent an ileostomy revision for stomal retraction.

Tissue Collection

Paired human small intestine samples were obtained at the time of small intestinal anastomosis after ileostomy from pathology specimens that otherwise would have been discarded. Ileostomy reversal occurred at least 7 weeks after their primary surgery. Proximal samples, obtained from the resected ileostomy margin that remained exposed to enteral nutrition before reversal, was referred to as fed. Samples obtained from the distal segment of ileum (either a Hartmann's pouch or mucus fistula), which were diverted from enteric feeding, were designated as unfed (Figure 1*A*). For fed and unfed samples, tissue was obtained within 1–2 cm of the proximal stoma (fed) and distal diverted (unfed) intestine. Both samples were placed immediately in saline on ice at the time of surgery. Specimens were divided into full-thickness sections for immediate storage in (1) 10% buffered formalin for paraffin-embedded blocks and sections, (2) RNAlater for RNA analyses (Life Technologies, NY) and snap frozen at -80°C, or (3) fresh frozen at -80°C for protein assays. Analyses were limited to the quantity of tissue available for individual specimens.

Histologic Quantification

H&E images were captured at 10× magnification by light microscope (DM 1000; Leica, Wetzlar, Germany) and quantified using ImageJ software (imagej.nih.gov; National Institutes of Health, Bethesda, MD). A blinded, trained observer analyzed only sections with full-thickness, non-obliqued epithelium. For patients with high-quality epithelium, a minimum of 10 villi and crypts from 2 different sections were quantified.

Immunofluorescence Microscopy

Sections (5 μm) of paraffin-embedded tissue were deparaffinized in Histochoice (Sigma-Aldrich, St. Louis, MO) and rehydrated in a graded ethanol series. Heat-induced antigen retrieval was performed with either a citrate-based pH 6.0 solution or a TRIS-based pH 9.0 antigen unmasking solution (Vector Laboratories, Inc, Burlingame, CA). Sections were blocked with 2% goat serum (Sigma-Aldrich, St. Louis, MO) and incubated with primary antibody (Table 3) overnight at 4°C. Secondary antibodies (Table 3) were incubated at room temperature for 1 hour.

For staining of LGR5 protein expression, we performed the protocol as reported by Dame et al.[23] Briefly, sections first were blocked with 3% hydrogen peroxide, followed by a donkey serum block. After incubation with primary antibody overnight, sections were incubated with biotinylated secondary antibody for 1 hour, then Vectastain Elite ABC Reagent (Vector Laboratories). Signal then was developed with tyramide signal amplification reagent (Dako, Carpinteria, CA) followed by fluorescein-conjugated streptavidin (Jackson ImmunoResearch Laboratories, Inc, West Grove, PA) for 30 minutes.

All slides were mounted in Vectashield with 4′,6-diamidino-2-phenylindole (Vector Laboratories) and imaged on an upright Leica DM5500B immunofluorescence microscope using Leica Suite Advanced Fluorescence (LAS AF) 6000 software. Positive cells then were quantified by a blinded, trained observer. Quantification of immunofluorescence was obtained by evaluating a minimum of 10 villi or crypts per sample from more than 6 different fields of view.

RNA Sequencing and Analysis

Total RNA was extracted using TRIzol reagent (Life Technologies) followed by Qiagen column purification with on-column DNAse digestion (Qiagen, Valencia, CA). RNA concentration was measured with Nanodrop (ThermoFisher Scientific, Waltham, MA).

Total RNA from 5 paired samples were selected to make complementary DNA libraries for RNA sequencing. RNA integrity was determined using a bioanalyzer (Agilent Technologies, Santa Clara, CA). All samples had an RNA integrity number of at least 7. Before library construction, samples were spiked with Ex-Fold External RNA Controls Consortium controls (Ambion, Foster City, CA). Mix 1 was added to RNA from fed intestine and mix 2 was added to RNA from unfed intestine. Libraries initially were sequenced to 10 million reads for power analysis via the Scotty algorithm.[24] Based on the results of the power analysis, libraries then underwent deep sequencing to 40 million base pairs. Sequences were assayed for quality using FastQC,[25] and adapter sequences as well as poor-quality sequences were removed with Trimmomatic.[26] By using ENCODE

Table 1. Patient Characteristics

Patient	Sex	Diagnosis	Gestational age, *wk*	Birth weight, *kg*	Age at resection, *wk*	Weight at resection, *kg*	Location of resection	Amount resected, *cm*	Diversion duration, *wk*	Nutrition after resection	Age at reversal, *mo*	Weight at reversal, *kg*	Weight gain, %	Nutrition after reversal	Ostomy complications	Postreversal complications	Comorbidities
A	F	NEC	25 4/7	0.770	2.0	0.750	Ileum: 7.5 cm from ICV	4	9.0	TPN + formula until ostomy reversal	2	1.785	138.00	TPN	None	Anastomotic leak	CLD, IVH, ROP, cholestasis of PN
B	F	FIP	24	0.700	2.5	0.835	Ileum: 5.0 cm from ICV	2	19.0	TPN + formula first 6 wk, then full formula	5	2.93	250.90	TPN until POD 5, formula started POD 6	Peristomal hernia without obstruction	None	CLD, IVH, ROP
C	F	FIP	24 5/7	0.705	5.0	1.040	Ileum: 15 cm from ICV	7	13.5	TPN + formula/BM until ostomy reversal	4.5	3.20	207.69	TPN until POD 23, formula started POD 7	None	Ileus	CLD, BPD, anemia, PS, ROP
D	F	FIP	28	0.810	1.0	0.800	Ileum: 45 cm from ICV	4	11.5	TPN + formula/BM until ostomy reversal	2	2.655	231.88	TPN until POD 27, formula started POD 18	Peristomal abscess	Ileus	CLD, PDA, anemia
E	M	NEC	26 3/7	0.900	1.5	0.900	Mid-ileum	1.5	31.0	TPN + formula first 4 wk, then full formula	7.5	5.1	466.67	TPN POD 8–11, formula started POD 10	None	None	PDA, ROP, GERD, apnea, anemia
F	M	FIP	26	0.810	1.0	0.810	Mid-ileum	9	15.0	TPN + formula until ostomy reversal	4	2.675	230.25	TPN until POD 15, formula started POD 10	None	Wound infection	Twin, CLD, PDA, cholestasis of PN
G	F	NEC	35	2.240	4.0	3.550	Ileum: 15 cm from ICV	20	7.0	TPN + formula until ostomy reversal	2.5	3.62	1.97	TPN until POD 14, formula started POD 5	Peristomal hernia without obstruction	None	Twin, rotavirus, thrombosis
H	M	FIP	25 1/7	0.655	1.0	0.680	Ileum just proximal to ICV	0	13.0	TPN + fortified BM/formula until ostomy reversal	3	2.415	255.15	TPN until POD 14, formula started POD 7	None	Fulminant pneumatosis	CLD, meningitis, sepsis, osteopenia
I	M	NEC	25	0.760	1.0	0.900	Ileum: 2 cm from ICV	4	44.0	TPN + formula first 6 wk, then full formula	10	6.54	626.67	TPN until POD 74, formula started POD 37	Stomal retraction	Adenovirus diarrhea	CLD, PDA cerebrovascular shunt, sepsis
J	M	FIP	26	0.650	1.5	0.685	Ileum: 22 cm from ICV	2	16.0	TPN + BM until ostomy reversal	4	2.655	287.59	TPN until POD 11, BM started POD 5	Peristomal skin breakdown	None	CLD, IVH, anemia, osteopenia, ROP
K	M	FIP	25 1/7	0.885	1.5	0.995	Ileum	0	11.5	TPN + BM for first 4 wk, then full BM	13	3.012	202.71	TPN until POD 22, BM started POD 7	EC fistula, peristomal skin breakdown	None	CLD, ROP
L	M	FIP	22 6/7	0.487	1.0	0.470	Ileum	8	19.0	TPN + BM until ostomy reversal	20	2.95	527.66	TPN until POD 18, BM started POD 10	None	Urosepsis, pneumonia	PDA, sepsis, ROP
M	F	FIP	24 5/7	0.705	5.0	1.040	Ileum	7	13.5	TPN + formula/BM until ostomy reversal	8	3.20	207.69	TPN until POD 26, formula started POD 7	None	Ileus	CLD, BPD, ROP, anemia, PS

Table 1. Continued

Patient	Sex	Diagnosis	Gestational age, *wk*	Birth weight, *kg*	Age at resection, *wk*	Weight at resection, *kg*	Location of resection	Amount resected, *cm*	Diversion duration, *wk*	Nutrition after resection	Age at reversal, *mo*	Weight at reversal, *kg*	Weight gain, %	Nutrition after reversal	Ostomy complications	Postreversal complications	Comorbidities
N	M	NEC	38 2/7	3.625	0.5	4.015	Ileum	4	48	TPN + formula for first 2 wk, then full formula until ostomy reversal	11	7.3	81.82	Formula started POD 5	Peristomal skin breakdown	None	Trisomy 21, HD, PDA, ASD
O	F	NEC	23	0.555	4.0	0.700	Ileum just proximal to ICV	15	18.5	Intermittent TPN + formula until ostomy reversal	5	3.185	355.00	TPN until POD 5, formula started POD 5	None	None	ROP

NOTE. Patient characteristics were obtained from medical records on consented patients who met criteria for the study.
ASD, atrial septal defect; BM, breast milk; BPD, bronchopulmonary dysplasia; CLD, chronic lung disease; EC, enterocutaneous; FIP, focal intestinal perforation; GERD, gastroesophageal reflux disease; HD, Hirschprung disease; ICV, ileocecal valve; IVH, intraventricular hemorrhage; PDA, patent ductus arteriosus; PN, parenteral nutrition; POD, postoperative day; PS, pulmonary stenosis; ROP, retinopathy of prematurity; TPN, total parenteral nutrition.

recommended parameters,[27] the remaining high-quality sequences were aligned using the RNA-star short-read aligner to the Gencode human genome version 23,[28] which corresponds to the Genome Research Consortium human genome version GRCh38.p3 (Genome Reference Consortium). Read counts per transcript were obtained using the HTSeq-count Python script.[29] Reads per kilobase per million mapped reads were generated using the edgeR[30] R/Bioconductor software package.[31] Relative log expression graphs and principle component graphs were generated using the plotting functions of the EDASeq R/Bioconductor software package.[32]

Differential gene expression was analyzed based on the Ex-Fold External RNA Controls Consortium probes with the Remove Unwanted Variation R/Bioconductor software package[33] combined with edgeR.[30] Genes with a false-discovery rate–corrected *P* value less than .05 were considered significant. Gene Ontology enrichment analysis for biological pathways was performed with the Gene Ontology stats R/Bioconductor software[34] and Gene Ontology Consortium (geneontology.org). Ontologic trees were created with BiNGO through Cytoscape.[35] A threshold of a $\log_2$ fold change $\geq$1.5 was selected for choosing genes of interest for further evaluation.

RNA sequencing raw data and processed data were deposited in the National Center for Biotechnology Information (NCBI) Gene Expression Omnibus. They can be accessed through GEO series accession number GSE82147. The top 100 up-regulated and down-regulated genes have been provided (Table 2).

For comparison of our RNA sequencing data with previously published RNA sequencing analysis of intestine with active NEC,[36] all differentially expressed genes with a *P* value less than .05 were downloaded with published fold changes. Pathway analyses were performed as described earlier. Human genes involved in pathways of interest were identified from Gene Ontology human annotation lists. Overlapping pathways and genes were compared to determine depth of similarity.

Quantitative Real-Time Polymerase Chain Reaction

Quantitative real-time polymerase chain reaction (PCR) was performed on several genes of interest to validate the RNA sequencing data. Primers (Table 4) were designed on the Roche (Indianapolis, IN) website (lifescience.roche.com) and purchased from Eurofins Operon (www.operon.com). A total of 1 μg of RNA was reverse-transcribed into complementary DNA with the iScript Reverse Transcription Supermix for real-time-PCR (Bio-Rad, Hercules, CA). Quantitative PCR (qPCR) was run in 96-well plates with SYBR Green (Roche) and analyzed with Roche Lightcycler 480 software release 1.5.0. Expression levels were calculated by the comparative threshold cycle method with delta delta threshold cycle values normalized to human glyceraldehyde-3-phosphate dehydrogenase.

PCR validation first was performed on the same 5 paired samples that underwent RNA sequencing analysis. If a

Table 2. Primary and Secondary Antibodies

Antibody	Species	Company	Catalog no	Dilution
Primary				
Mucin 2 (MUC2)	Rabbit	Santa Cruz Biotechnology (Dallas, TX)	sc-15334	1:100
Chromogranin A (CHGA)	Rabbit	Abcam (Cambridge, MA)	ab15160	1:100
Lysozyme (LYZ)	Rabbit	Dako Cytomation	A0099	1:100
E-cadherin (E-CAD)	Mouse	BD Transduction (San Jose, CA)	610181	1:100
Ki67	Rabbit	Thermo Scientific (Waltham, MA)	RM-9106-S1	1:100
Proliferating cell nuclear antigen	Mouse	Vector Laboratories	VP-P980	1:100
Cleaved caspase 3 (CC3)	Rabbit	Cell Signaling Technologies (Danvers, MA)	9661	1:50
LGR5	Rabbit	Miltenyi (San Diego, CA)	130-104-945	1:200
Phosphorylated STAT3 (pSTAT3)	Rabbit	Cell Signaling Technologies	9145	1:1000
STAT3	Rabbit	Cell Signaling Technologies	4904	1:1000
Actin (clone AC-15)	Mouse	Sigma (St. Louis, MO)	A1978	1:10,000
OLFM4	Rabbit	Abcam	AB85046	1:200
SOX9	Rabbit	Millipore (Billerica, MA)	AB5535	1:200
Secondary				
Alexa Fluor anti-rabbit 488	Goat	Life Technologies (Carlsbad, CA)	Z25302	1:200
Alexa Fluor anti-rabbit 555	Goat	Life Technologies	A21429	1:200
Biotinylated anti-rabbit	Goat	Jackson ImunoResearch (West Grove, PA)	111-066-047	1:1000
DTAF-conjugated streptavidin		Jackson ImunoResearch	016-101-084	1:500
IRDye 680LT anti rabbit	Donkey	LI-COR (Lincoln, NE)	926-68023	1:10,000
IRDye 800CW anti-mouse	Donkey	LI-COR	926-32212	1:10,000

NOTE. The name, source, catalog number, and dilution are provided for the primary and secondary antibodies included in the study.
DTAF, dichlorotriazinyl aminofluorescein.

significant fold change was found on qPCR, 3 additional pairs were evaluated by PCR. Outliers were identified with the ROUT test, Q = 0.1%, and excluded from statistical analysis. This resulted in 6–7 pairs included in the PCR analyses.

In Situ Hybridization

The RNAscope 2.5 HD Reagent Kit-RED (322350; Advanced Cell Diagnostics, Newark, CA) was performed on 5-μm, formalin-fixed, paraffin-embedded sections according to the manufacturer's instructions. The RNAscope probes used were LGR5 (NM_003667.2, region 560–1589, cat no: 311021) and negative control probe DapB (EF191515, region 414–862, cat no: 310043). Crypt expression of *LGR5* messenger RNA (mRNA) was quantified according to a modified 5-grade scoring system recommended by the manufacturer (0 = no staining or <1 dot to every 10 cells [63× magnification]; 1 = 1–3 dots/cell [visible at 40–63× magnification]; 2 = 4–10 dots/cell, very few dot clusters [visible at 40–63× magnification]; 3 = more than 10 dots/cell, <10% positive cells have dot clusters [visible at 40–63× magnification]; and 4 = >10 dots/cell). More than 10% positive cells have dot clusters (visible at 40–63× magnification). At least 15 crypts from 4 individual patient samples were quantified.

Western Blot

Protein was extracted from 5 pairs of homogenized full-thickness samples of intestine in RIPA buffer, protease inhibitor cocktail (Roche), and phosphatase inhibitor cocktail (Roche). Concentrations were assessed with a BCA protein assay (ThermoFisher Scientific). Samples were run on 4%–12% Bis-Tris Plus gels (ThermoFisher Scientific) in Bolt MES sodium dodecyl sulfate running buffer (ThermoFisher Scientific). After blocking with Odyssey blocking buffer (LI-COR, Lincoln, NE), primary antibodies were incubated overnight at 4°C (Table 3). Secondary antibodies (Table 3) were incubated at room temperature for 1 hour. Blots then were scanned digitally and densitometry-quantified with Image-Studio (LI-COR). Densitometry was quantified relative to actin.

Statistical Analyses

Histologic measurements and cell counts were compared with paired 2-tailed Wilcoxon rank-sum tests. To confirm differences noted on RNA sequencing, PCR gene expression values were compared with a paired 1-tailed Wilcoxon rank-sum test. All calculations were performed on Prism (GraphPad Software, San Diego, CA). Values are expressed as medians (95% confidence interval). *P* values less than .05 were considered significant. Outliers were identified with the ROUT test, Q = 0.1%, and excluded from statistical analysis.[37]

Results

Mechanoluminal Deprivation Decreases Intestinal Epithelial Proliferation

Morphometry from pairs with high-quality epithelium was compared to define histologic changes associated with loss of mechanoluminal stimulation. In unfed intestine, villi were 10%–66% shorter and crypts were 22%–62% deeper (Figure 2*A–D*) (n = 7; *P* = .02). The muscularis mucosae was 5%–55% thinner (Figure 1*C*) (n = 5; *P* = .03), although the majority of stromal elements within the unfed limb by H&E analysis remained similar to fed intestine (Figure 1*B*). There was no difference noted in crypt width or density, defined as the number of crypts per millimeter of tissue. There was no significant correlation between the length of

Table 3. Top 100 Up- and Down-Regulated Genes in Unfed Small Intestine

Gene name	Description	logFC	LR	*P* value	Ensembl gene ID
FMO1	Flavin containing monooxygenase 1	1.935156001	74.80308156	5.20085E-18	ENSG00000010932
UPK3A	Uroplakin 3A (source: HGNC symbol)	2.147520087	46.60854851	8.66813E-12	ENSG00000100373
CXCL5	Chemokine (C-X-C motif) ligand 5	-2.733639395	41.69682868	1.06582E-10	ENSG00000163735
RNF224	Ring finger protein 224	1.839210925	41.87209741	9.74433E-11	ENSG00000233198
CYSRT1	Cysteine-rich tail protein 1	1.720249115	39.9409415	2.61759E-10	ENSG00000197191
SLC5A12	Solute carrier family 5 (sodium/monocarboxylate cotransporter), member 12	2.132807939	38.74458626	4.83048E-10	ENSG00000148942
SULT2A1	Sulfotransferase family, cytosolic, 2A, dehydroepiandrosterone-preferring, member 1	2.097488909	37.82205594	7.75006E-10	ENSG00000105398
MRO	Maestro	1.848607121	36.97909256	1.19403E-09	ENSG00000134042
LINC01595	Long intergenic nonprotein coding RNA 1595	2.165402806	36.06166015	1.91171E-09	ENSG00000259108
SHBG	Sex hormone-binding globulin	1.738789918	35.47000772	2.59008E-09	ENSG00000129214
SLC23A1	Solute carrier family 23 (ascorbic acid transporter), member 1	1.603537606	35.15428148	.000000003	ENSG00000170482
SLC34A3	Solute carrier family 34 (type II sodium/phosphate cotransporter), member 3	1.537065735	34.51159913	4.23719E-09	ENSG00000198569
PDZK1	PDZ domain containing 1	1.585707896	34.29271495	4.74153E-09	ENSG00000174827
TREH	Trehalase (brush-border membrane glycoprotein)	1.194202148	33.81359331	6.06536E-09	ENSG00000118094
SULT1C2	Sulfotransferase family, cytosolic, 1C, member 2	1.907549377	33.14195314	8.56702E-09	ENSG00000198203
ENPP7	Ectonucleotide pyrophosphatase/phosphodiesterase 7	1.300165718	32.59690058	1.13395E-08	ENSG00000182156
F7	Coagulation factor VII (serum prothrombin conversion accelerator)	1.780260275	31.79235485	1.71567E-08	ENSG00000057593
CYP4F2	Cytochrome P450, family 4, subfamily F, polypeptide 2	1.683482981	31.31912349	2.18913E-08	ENSG00000186115
SLC13A1	Solute carrier family 13 (sodium/sulfate symporter), member 1	2.538985085	30.81618591	2.83662E-08	ENSG00000081800
SLC5A9	Solute carrier family 5 (sodium/sugar cotransporter), member 9	1.538317273	30.90810275	2.7054E-08	ENSG00000117834
PRKG2	Protein kinase, cGMP-dependent, type II	1.27808205	30.94340641	2.65663E-08	ENSG00000138669
RP11-798K3.2	NA	1.855803844	30.7019997	3.00855E-08	ENSG00000259347
FRMD1	FERM domain containing 1	1.696220028	30.15783587	3.98275E-08	ENSG00000153303
NAALADL1	N-acetylated α-linked acidic dipeptidase-like 1	1.672980254	30.09099621	4.12241E-08	ENSG00000168060
MS4A8	Membrane-spanning 4-domains, subfamily A, member 8	1.779882861	29.92631817	4.4878E-08	ENSG00000166959
FADS6	Fatty acid desaturase 6	1.921798418	29.9963597	4.32858E-08	ENSG00000172782
SLC7A9	Solute carrier family 7 (amino acid transporter light chain, bo,+ system), member 9	1.481271455	29.75955747	4.89089E-08	ENSG00000021488
CDHR5	Cadherin-related family member 5	1.515548333	29.50960252	5.56404E-08	ENSG00000273572
CEL	Carboxyl ester lipase	1.634979875	28.99145378	7.26983E-08	ENSG00000170835
NAT8	N-acetyltransferase 8 (GCN5-related, putative)	2.675738291	28.71017357	8.4061E-08	ENSG00000144035
ATP13A4	ATPase type 13A4	1.939358607	28.12477638	1.1374E-07	ENSG00000127249
UNC93A	Unc-93 homolog A (*Caenorhabditis elegans*)	1.601007557	28.04197919	1.18712E-07	ENSG00000112494
SLC2A2	Solute carrier family 2 (facilitated glucose transporter), member 2	1.556431458	27.87085693	1.29688E-07	ENSG00000163581
TMIGD1	Transmembrane and immunoglobulin domain-containing 1	1.967330736	27.70509208	1.4129E-07	ENSG00000182271
TFEC	Transcription factor EC	1.321562424	27.57164133	1.51382E-07	ENSG00000105967
CUBN	Cubilin (intrinsic factor-cobalamin receptor)	2.341955896	27.18194662	1.8518E-07	ENSG00000107611

Table 3. Continued

Gene name	Description	logFC	LR	*P* value	Ensembl gene ID
SLC19A3	Solute carrier family 19 (thiamine transporter), member 3	1.552887155	27.26057746	1.778E-07	ENSG00000135917
SMLR1	Small leucine-rich protein 1	1.612876682	27.21140528	1.8238E-07	ENSG00000256162
NNMT	Nicotinamide N-methyltransferase	-1.472271231	26.94985142	2.08803E-07	ENSG00000166741
NAT8B	N-acetyltransferase 8B (GCN5-related, putative, gene/pseudogene)	1.718975423	26.9959476	2.03882E-07	ENSG00000204872
SLC28A1	Solute carrier family 28 (concentrative nucleoside transporter), member 1	1.407436527	26.62926909	2.46481E-07	ENSG00000156222
AC007325.2	NA	1.46829846	26.64878695	.000000244	ENSG00000277196
GGT1	γ-Glutamyltransferase 1	1.080943383	26.48751824	2.65246E-07	ENSG00000100031
TRPM6	Transient receptor potential cation channel, subfamily M, member 6	1.828527681	26.32603584	2.88375E-07	ENSG00000119121
KHK	Ketohexokinase (fructokinase)	1.251604031	26.35745455	2.83722E-07	ENSG00000138030
SLC6A4	Solute carrier family 6 (neurotransmitter transporter), member 4	1.399303921	25.97462634	3.45934E-07	ENSG00000108576
SLC28A2	Solute carrier family 28 (concentrative nucleoside transporter), member 2	2.441573348	25.9860024	3.43902E-07	ENSG00000137860
ENPP3	Ectonucleotide pyrophosphatase/phosphodiesterase 3	1.084760034	26.01060946	3.39546E-07	ENSG00000154269
TMEM236	Transmembrane protein 236	1.492276653	25.93225942	3.5361E-07	ENSG00000148483
NR1H4	Nuclear receptor subfamily 1, group H, member 4	1.530681737	25.66165786	4.0683E-07	ENSG00000012504
COL2A1	Collagen, type II, α 1	2.7427092	25.57237858	4.26095E-07	ENSG00000139219
DPEP1	Dipeptidase 1 (renal)	2.012092029	25.51498355	.000000439	ENSG00000015413
SLC16A10	Solute carrier family 16 (aromatic amino acid transporter), member 10	1.574547146	25.44844819	4.54363E-07	ENSG00000112394
CLIC5	Chloride intracellular channel 5 [	1.133191008	25.28347044	4.94932E-07	ENSG00000112782
PRLR	Prolactin receptor	1.441337236	25.30981848	4.88217E-07	ENSG00000113494
MCOLN3	Mucolipin 3	1.595364418	25.21959734	5.11597E-07	ENSG00000055732
RP11-1193F23.1	NA	2.585443625	25.20976053	5.14213E-07	ENSG00000279024
PKIB	Sp8 transcription factor	6.674019267	25.17393696	5.23854E-07	ENSG00000164651
MAMDC4	MAM domain containing 4	1.277939128	24.86218203	6.15787E-07	ENSG00000177943
SLC3A1	Solute carrier family 3 (amino acid transporter heavy chain), member 1	1.781625122	24.80772832	6.3343E-07	ENSG00000138079
PKIB	Protein kinase (cAMP-dependent, catalytic) inhibitor β	1.549061572	24.60352117	7.04229E-07	ENSG00000135549
CYP3A4	Cytochrome P450, family 3, subfamily A, polypeptide 4	1.922951569	24.62844524	6.9518E-07	ENSG00000160868
CDHR5	Cadherin-related family member 5	1.430921311	24.46118573	7.5822E-07	ENSG00000099834
SOAT2	Sterol O-acyltransferase 2	1.220274465	24.30393855	8.22707E-07	ENSG00000167780
SFRP5	Secreted frizzled-related protein 5	1.289605732	24.05353528	9.36941E-07	ENSG00000120057
DAB1	Dab, reelin signal transducer, homolog 1	1.317550733	24.100991	9.14132E-07	ENSG00000173406
LRRC19	Leucine-rich repeat containing 19	1.489115345	24.05615315	9.35668E-07	ENSG00000184434
TYRP1	Tyrosinase-related protein 1	-1.664137392	23.96832679	9.79336E-07	ENSG00000107165
CCDC108	Coiled-coil domain containing 108	2.035404412	23.98451824	9.71135E-07	ENSG00000181378
TRHDE-AS1	TRHDE antisense RNA 1	2.045816171	23.98498662	9.70898E-07	ENSG00000236333
AQP7	Aquaporin 7	1.601418775	23.74146929	1.10183E-06	ENSG00000165269
MYO7A	Myosin VIIA	1.042545085	23.61253694	1.17817E-06	ENSG00000137474
SLC26A2	Solute carrier family 26 (anion exchanger), member 2	1.088822376	23.62142755	1.17274E-06	ENSG00000155850

Table 3. Continued

Gene name	Description	logFC	LR	*P* value	Ensembl gene ID
SLC30A2	Solute carrier family 30 (zinc transporter), member 2	1.335008616	23.60508117	1.18275E-06	ENSG00000158014
SMIM24	Small integral membrane protein 24	1.25301892	23.47494696	1.26551E-06	ENSG00000095932
RORC	RAR-related orphan receptor C	1.621731103	23.41211242	1.30753E-06	ENSG00000143365
CLEC4F	C-type lectin domain family 4, member F	1.905689525	23.13627604	1.50916E-06	ENSG00000152672
FOLH1	Folate hydrolase (prostate-specific membrane antigen) 1	1.593863663	23.09609472	.000001541	ENSG00000086205
PGC	Progastricsin (pepsinogen C)	-1.923972415	22.99096472	1.62765E-06	ENSG00000096088
FOSL1	FOS-like antigen 1	-2.400350289	22.87060113	1.73282E-06	ENSG00000175592
ABCC6	ATP-binding cassette, subfamily C (CFTR/MRP), member 6	1.701645886	22.74240918	1.85234E-06	ENSG00000091262
SLC52A1	Solute carrier family 52 (riboflavin transporter), member 1	1.330488729	22.76413548	1.83152E-06	ENSG00000132517
ERICH4	Glutamate-rich 4	1.152189244	22.77999852	1.81646E-06	ENSG00000204978
PNLIPRP2	Pancreatic lipase-related protein 2	1.430493624	22.75890815	1.83651E-06	ENSG00000266200
ASAH2	N-acylsphingosine amidohydrolase (nonlysosomal ceramidase) 2	1.367297002	22.67467775	1.9188E-06	ENSG00000188611
PDZD7	PDZ domain containing 7	1.19335086	22.6056947	1.98894E-06	ENSG00000186862
DCSTAMP	Dendrocyte-expressed 7 transmembrane protein	4.290165257	22.35510009	2.2661E-06	ENSG00000164935
ABCG8	ATP-binding cassette, subfamily G (white), member 8	1.334210188	22.32450691	2.30249E-06	ENSG00000143921
RAB17	RAB17, member RAS oncogene family	1.246564272	22.24989867	2.39371E-06	ENSG00000124839
CA7	Carbonic anhydrase VII	1.453047121	22.28269301	2.35318E-06	ENSG00000168748
KCNH6	Potassium channel, voltage-gated eag-related subfamily H, member 6	1.685088587	22.25545876	2.38679E-06	ENSG00000173826
ESPN	Espin	1.133210251	22.06396747	2.63714E-06	ENSG00000187017
C10orf99	Chromosome 10 open reading frame 99	2.465624328	22.05917803	2.64373E-06	ENSG00000188373
CLDN23	Claudin 23	1.045566126	22.05403209	2.65082E-06	ENSG00000253958
SLC26A3	Solute carrier family 26 (anion exchanger), member 3	1.494972698	22.01805961	.000002701	ENSG00000091138
BTNL3	Butyrophilin-like 3	1.265622259	21.86960556	2.9182E-06	ENSG00000168903
B4GALNT2	β-1,4-N-acetyl-galactosaminyl transferase 2	2.203101248	21.8177065	2.9982E-06	ENSG00000167080
MEP1B	Meprin A, β	1.442428396	21.74734893	3.11019E-06	ENSG00000141434
ENTPD8	Ectonucleoside triphosphate diphosphohydrolase 8	1.275503513	21.74791285	3.10928E-06	ENSG00000188833
OSBP2	Oxysterol binding protein 2	1.073037668	21.62906423	.000003308	ENSG00000184792

NOTE. RNA sequencing analysis identified the top 100 up- and down-regulated genes that were affected by prolonged absence of mechanoluminal stimulation in human patients with ileostomies.
ATP, adenosine triphosphate; cAMP, cyclic adenosine monophosphate; CFTR/MRP, cystic fibrosis transmembrane conductance regulator/multidrug resistance-associated protein; cGMP, cyclic guanosine monophosphate; EC, classic E basic helix-loop-helix protein; FERM, 4.1 protein/ezrin/radixin/moesin; FOS, Fos proto-oncogene, AP-1 transcription factor subunit; GCN5, gene control of amino acid synthesis protein 5-like 2; HGNC, HUGO Gene Nomenclature Committee; MAM, meprin/A-5 protein/ receptor protein-tyrosine phosphatase mu; RAR, retinoic acid receptor; RAS, retrovirus-associated DNA sequences; TRHDE, thyrotropin releasing horomone degrading enzyme.

Table 4. qPCR Primer List

Gene	Primer sequence
LGR5	F: GCCCTTCCACGATGCCAAAG R: GGCTGGGGCTCACCTGAAG
CCND1	F: GCCGAGAAGCTGTGCATC R: CCACTTGAGCTTGTTCACCA
C-MYC	F: GCTGCTTAGACGCTGGATTT R: TAACGTTGAGGGGCATCG
REG1b	F: GCCTCCATGACCCAAAAA R: TTGCACAGTAGCCAGCATTAG
IL1B	F: TACCTGTCCTGCGTGTTGAA R: TCTTTGGGTAATTTTTGGGATCT
COL2A1	F: GTGAACCTGGTGTCTCTGGTC R: TTTCCAGGTTTTCCAGCTTC
NAT8	F: GGACCAGGGCTACAGTGAAGT R: TGGTAGAGGGCCATAGCAGA
IL22	F: CAACAGGCTAAGCACATGTCA R: ACTGTGTCCTTCAGCTTTTGC
FMO1	F: TTGGCACCAGAAATTACAAGAG R: TTCCAGACAGCACTTGATGG

NOTE. Forward (F) and reverse (R) primer sequences for genes of interest in the study are provided.

time of diversion and the percentage difference in villus height and crypt depth. There was not any difference between infants who received breast milk vs formula, or between infants who weaned off total parenteral nutrition preoperatively vs those who did not. There was no correlation with the duration of total parenteral nutrition after ileostomy reversal and the percentage difference in villus height and crypt depth.

The overall decrease in villus height was not associated with a measurable difference in differentiated epithelial cell types in the villus. There was no difference in the number of MUC2+ goblet cells (Figure 2*E*–*G*) (n = 5; $P = .19$) or chromagranin A+ enteroendocrine cells (Figure 2*H*–*J*) (n = 5; $P = .19$) per hemivillus between fed and unfed intestine, suggesting that enterocytes were fewer in number in unfed intestine. In the crypts, however, unfed intestine had significantly fewer LYZ+ Paneth cells (Figure 2*K*–*M*) (n = 6; $P = .03$).

Crypt proliferation and villus apoptosis then were examined to explain the differences in villus and crypt size. Ki67+ immunofluorescence staining showed a 0.6%–21% decrease in the percentage of proliferating cells in the crypt of unfed intestine (Figure 2*N*–*P*) (n = 5; $P = .03$). Analysis of apoptosis by CC3+ staining showed that in both limbs, apoptosis was a rare event with no significant difference in the numbers (Figure 2*Q*–*S*) (n = 4; $P = .41$).

Absence of Mechanoluminal Stimulation in Diverted Small Intestine Is Associated With Increased Expression of Digestion, Metabolism, and Transport Genes

RNA sequencing genome-wide analysis (NCBI Gene Expression Omnibus, GSE82147) was performed on 5 pairs (patients F–J) to identify biological processes affected by the absence of mechanoluminal stimulation. The top 100 up-regulated and down-regulated genes were identified (Table 2). On principal component analysis of all sequenced genes, unfed limbs clustered more closely than fed limbs, although there still was overlap of the fed and unfed limbs (Figure 3*A*). Of the 22,007 genes sequenced, 648 had significant differences in expression between paired fed and unfed limbs, with a false-discovery rate corrected *P* value less than .05 (Figure 3*B*). This included protein-coding transcripts and non–protein-coding transcripts, for example, long non-codingRNA, processed and polymorphic pseudogenes. Eighty-five percent of these significantly different genes were up-regulated in the unfed limb. A total of 191 had a $\log_2$-fold change greater than 1.5 or less than -1.5. Validation of selected target genes (*LGR5*, *COL2A1*, *NAT8*, *FMO1*, *IL22*, *REG1B*, and *IL1B*) with qPCR confirmed significant differences in expression with high correlation between the RNA sequencing and qPCR data (Figure 3*C*) ($r > 0.9$; $P < .01$).

Significantly different genes were compared with the *Homo sapiens* gene annotations of biological processes in the Gene Ontology Consortium database to determine which processes were over-represented and which were under-represented. A process was over-represented if significantly more of our differently expressed genes annotated to that process than in the background database. In the unfed limb, Gene Ontology analysis of significantly up-regulated genes showed that digestion, nutrient transport, and absorption, particularly of fatty acids and cholesterol, were over-represented pathways (Figure 4*A* and Supplementary Table 1). Conversely, nucleic acid synthesis and transcription were under-represented pathways (Figure 4*B* and Supplementary Table 2). Significantly down-regulated genes were involved in immune system processes, inflammation, angiogenesis, cell proliferation, and apoptosis (Figure 4*C* and Supplementary Table 3). No processes were significantly under-represented by these down-regulated genes.

Enteric Diversion Increases LGR5 mRNA Expression and Alters Downstream Wnt/β-Catenin Target Genes in the Intestine Lacking Mechanoluminal Flow

Given the diminished villus height/crypt depth, reduced cellular division within the transit-amplifying zone, and broad decrease in cell proliferation genes in unfed intestine, we sought to elucidate the effect of mechanoluminal deprivation on the ISC population. Several ISC markers recently were identified for both proliferative, more damage-sensitive crypt-based cells (*LGR5*, *ASCL2*, *SOX9*, *OLFM4*, *MSI1*, and *SMOC2*) and a class of more damage-resistant +4 stem cells (*BMI1*, *LRIG1*, *HOPX*, and *TERT*).[38] Only *LGR5* mRNA had a more than 1.5 $\log_2$-fold change difference in expression on RNA sequencing analysis, with increased expression in the unfed limb (NCBI Gene Expression Omnibus GSE82147, $\log_2$-fold change = 1.68; $P = .01$). In situ hybridization confirmed increased expression of *LGR5* mRNA within ISCs within the crypts of unfed intestine compared with

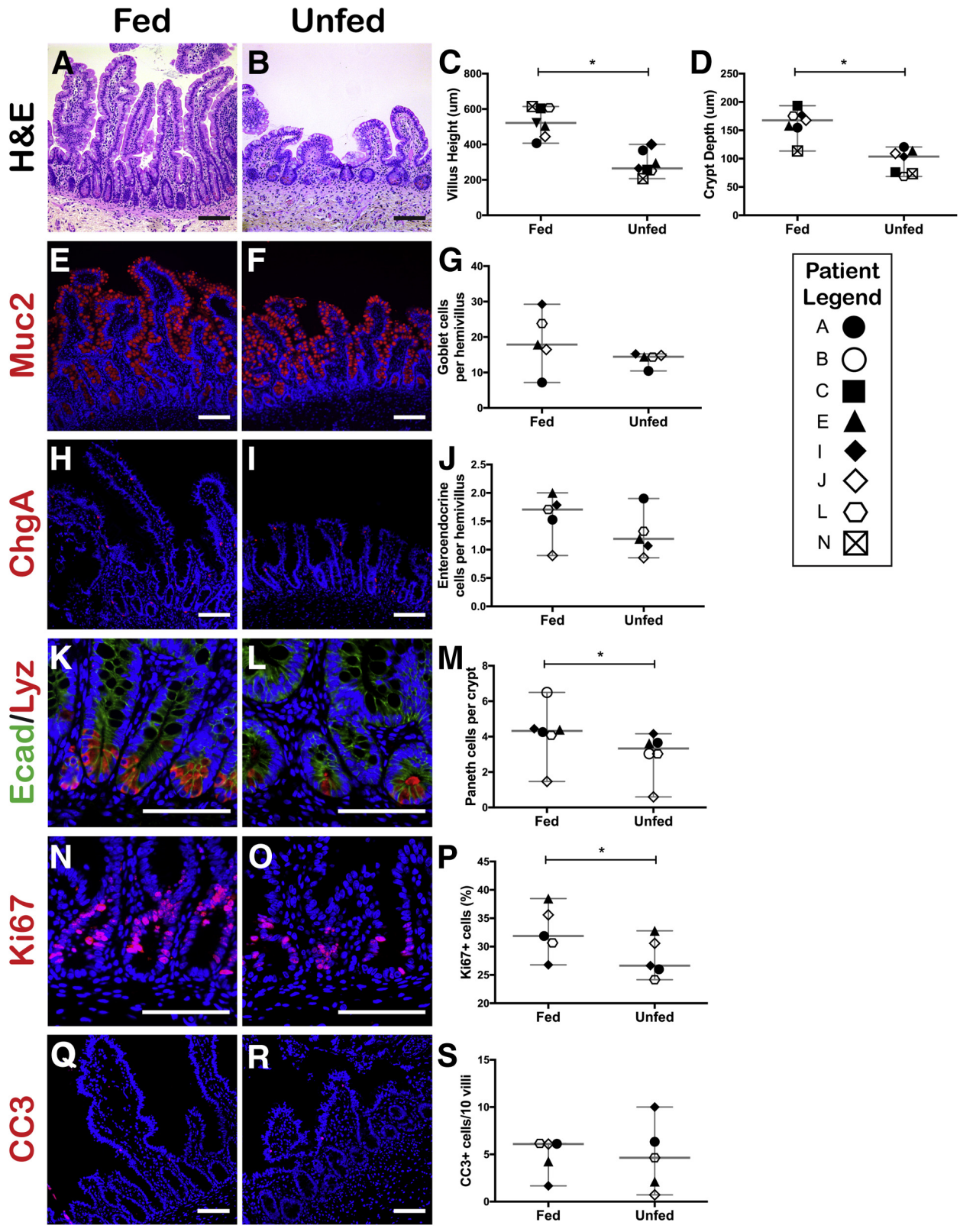

Figure 2. Absence of mechanoluminal stimulation decreases villus height, crypt depth, and crypt proliferation. (*A–D*) H&E staining and morphometric analysis of matched fed vs unfed intestine from each patient. (*E–S*) Immunofluorescence staining and quantification of (*E–G*) MUC2+ goblet cells per hemivillus, (*H–J*) chromagranin A (CHGA)+ enteroendocrine cells per hemivillus, (*K–M*) LYZ+ Paneth cells per crypt with E-cadherin (Ecad) counterstain, (*N–P*) percentage of Ki67+ cells in crypts, and (*Q–S*) CC3+ cells per 10 villi. Images are representative pairs from different patients (n = 5–7 pairs of intestine for quantification). Images were obtained on an upright Leica DM5500B immunofluorescence microscope using Leica Suite Advanced Fluorescence (LAS AF) 6000 software, processed with ImageJ software. *Scale bars*: 100 μm. *$P < .05$. *Grey bars* on plots indicate median with 95% confidence interval.

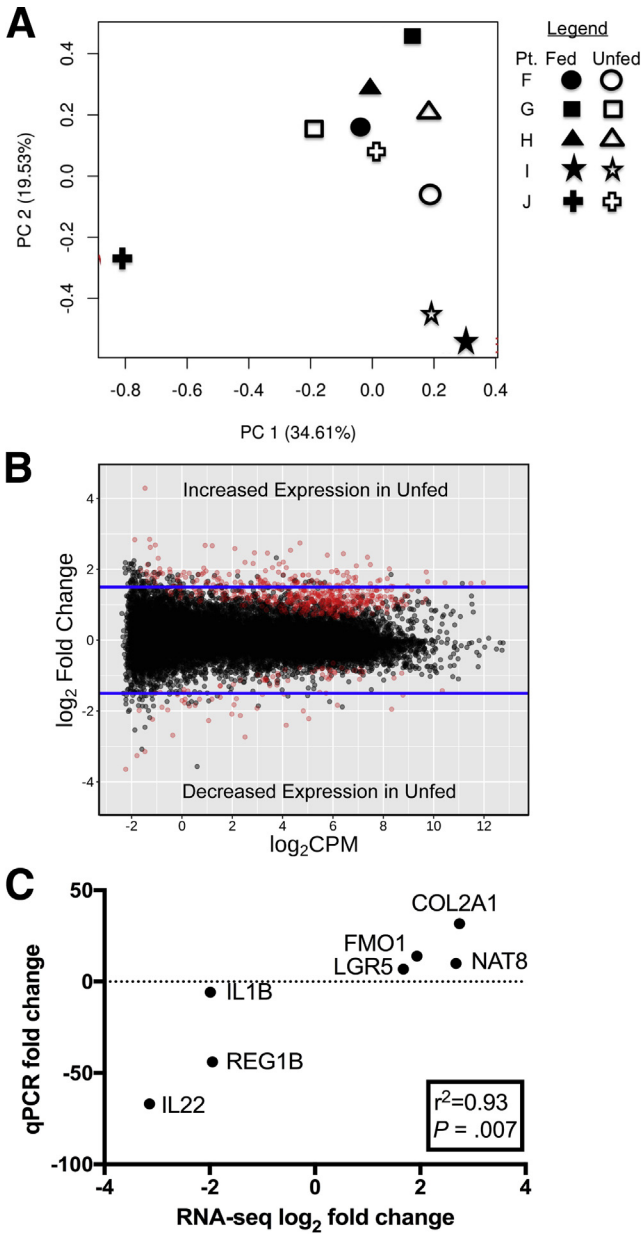

Figure 3. Genome-wide analysis of fed and unfed intestine shows significant changes in unfed intestine. (*A*) Principal component analysis of 5 matched unfed (white) and fed (black) intestinal pairs analyzed by RNA sequencing. Two principal components were analyzed with the percentage of variability explained by each component shown. (*B*) Volcano plot of sequenced genes. On the x-axis, $\log_2$ transformed counts per million (CPM) graphs the number of reads per gene. The average $\log_2$ transformed fold change of each gene is plotted on the y-axis with a positive fold change indicating increased expression in the unfed limb. Each *dot* represents 1 gene. *Red dots* are those with a false-discovery rate corrected *P* value < .05. Blue lines at y = 1.5 and -1.5 indicate the cut-off value chosen for meaningful fold change. (*C*) Correlation of RNA sequencing determined $\log_2$ fold changes with qPCR-based fold changes for 7 selected genes of interest.

the fed limb (Figure 5*A* and *B*) (n = 4; $P < .01$). qPCR confirmed a 1.9- to 22.9-fold change between pairs (Figure 5*C*) (n = 7; $P = .008$).

LGR5 regulates the Wnt/β-catenin pathway,[39] which promotes transcription of cell-cycle regulators *CCND1* and *MYC*. qPCR confirmed significantly increased mRNA expression for these genes in the unfed limb (Figure 5*C* and *D*) (n = 6; $P = .03$ for *CCND1* and $P = .02$ for *MYC*). Upstream of LGR5, previous studies have shown the importance of signal transducer and activator of transcription 3 (STAT3) function in the survival and proliferation in intestinal stem cells.[40,41] Furthermore, phosphorylation of STAT3 also induces expression of *CCND1* and *C-MYC*.[42] Consequently, Western blot analysis of STAT3 phosphorylation was performed and confirmed increased STAT3 phosphorylation in unfed intestine (Figure 5*F*) (n = 5; $P = .03$).

Mechanoluminal Deprivation Decreases Intestinal Stem Cell Populations

LGR5 had a more than 1.5 $\log_2$-fold change difference in expression on RNA sequencing analysis, with increased expression in the unfed limb (NCBI Gene Expression Omnibus, GSE82147). Immunofluorescence staining for LGR5 then was performed to localize LGR5 expression and quantify ISC. Positive immunofluorescence staining for LGR5 was found at the crypt bases in non-Paneth cells (Figure 6*A*–*F*). Although RNA sequencing analysis showed that *LGR5* mRNA expression was increased in the unfed limb, quantification of ISC actually showed 8%–37% fewer ISCs per crypt in unfed intestine (Figure 6*G*) (n = 5; $P = .03$). Co-staining with proliferative marker proliferating cell nuclear antigen (Figure 6*A*, *B*, *D*, and *E*) also showed that 1%–60% fewer LGR5+ cells were proliferating in unfed intestine (Figure 6*H*) (n = 5; $P = .03$).

Other ISCs showed changes in expression levels between fed and unfed intestine that were statistically significant; however, their $\log_2$-fold change difference was less than 1.5. *ASCL2* was up-regulated in unfed intestine (NCBI Gene Expression Omnibus GSE82147, $\log_2$-fold change = 1.49; $P = .005$), whereas *HOPX* ($\log_2$-fold change = -0.80; $P = .02$) and *LRIG1* (NCBI Gene Expression Omnibus GSE82147, $\log_2$-fold change = -0.43; $P = .05$) were down-regulated. *BMI1*, *OLFM4*, *TERT*, and *SOX9* remained unchanged. Given the discordance between mRNA expression and LGR5+ cell numbers in the distal unfed limb, we evaluated SOX9 (Figure 6*I* and *J*) and OLFM4 (Figure 6*L* and *M*) expression to determine if other ISCs were affected in a similar manner. In the unfed limb, 40%–56% fewer SOX9+ (Figure 6*K*) (n = 4; $P = .03$) and 22%–31% fewer OLFM4+ cell numbers (Figure 6*N*) (n = 4; $P = .03$) were identified.

Chronic Absence of Mechanoluminal Stimulation Is Associated With Increased Brush Border Function and Down-Regulation of Cell Proliferation, Inflammation, and Immune Process Genes

To further investigate differential regulation of biological processes in chronically diverted intestine lacking mechanoluminal flow, we investigated gene families important in brush-border structure and activity, stem cell pathways,

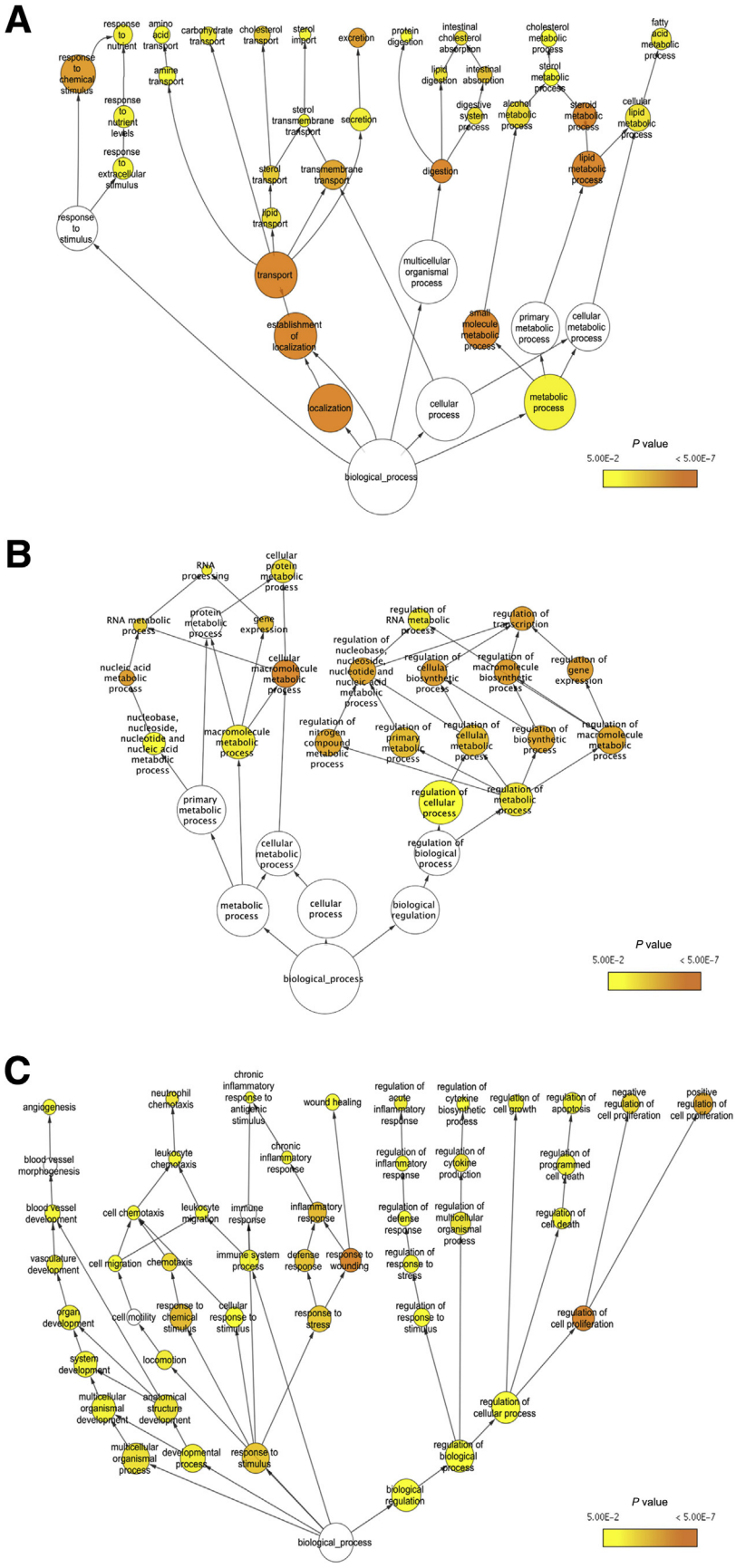

Figure 4. Gene Ontology enrichment analysis of genes up-regulated and down-regulated by absence of mechanoluminal stimulation indicates significantly affected biological processes. Gene Ontology (GO) analysis of up-regulated genes (*A*) over-represented and (*B*) under-represented by withdrawal of mechanoluminal stimulation and (*C*) down-regulated genes over-represented by the absence of mechanoluminal stimulation with a false-discovery rate corrected *P* value $<$ .05. Over-represented pathways are shown, with *circle size* proportional to the number of genes included in the GO term. *P* value is represented by the color scale. *Arrows* indicate hierarchical relationships with most generalized terms at the base.

immunologic function, and cell proliferation/death. Heatmap representation of these genes shows differential expression between the fed and unfed limbs (Figure 7*A*–*E*). Regarding the top 100 up-regulated and down-regulated genes in our data set, a vast majority were up-regulated genes intrinsic to brush-border enzymatic, transporter, or structural function (Table 2). Common brush-border enzymes TREH, MGAM, and SI, and transporters SLC15A1, SLC9A3, ABCG2, and ABCC2, were increased significantly in the unfed limb ($P < .001$) (Figure 7*A*).

Although *LGR5* was the only stem cell marker gene with a $\log_2$-fold change greater than 1.5, we further characterized the changes in RNA expression among common ISCs and downstream targets (Figure 7*B*). *LGR5* (NCBI Gene

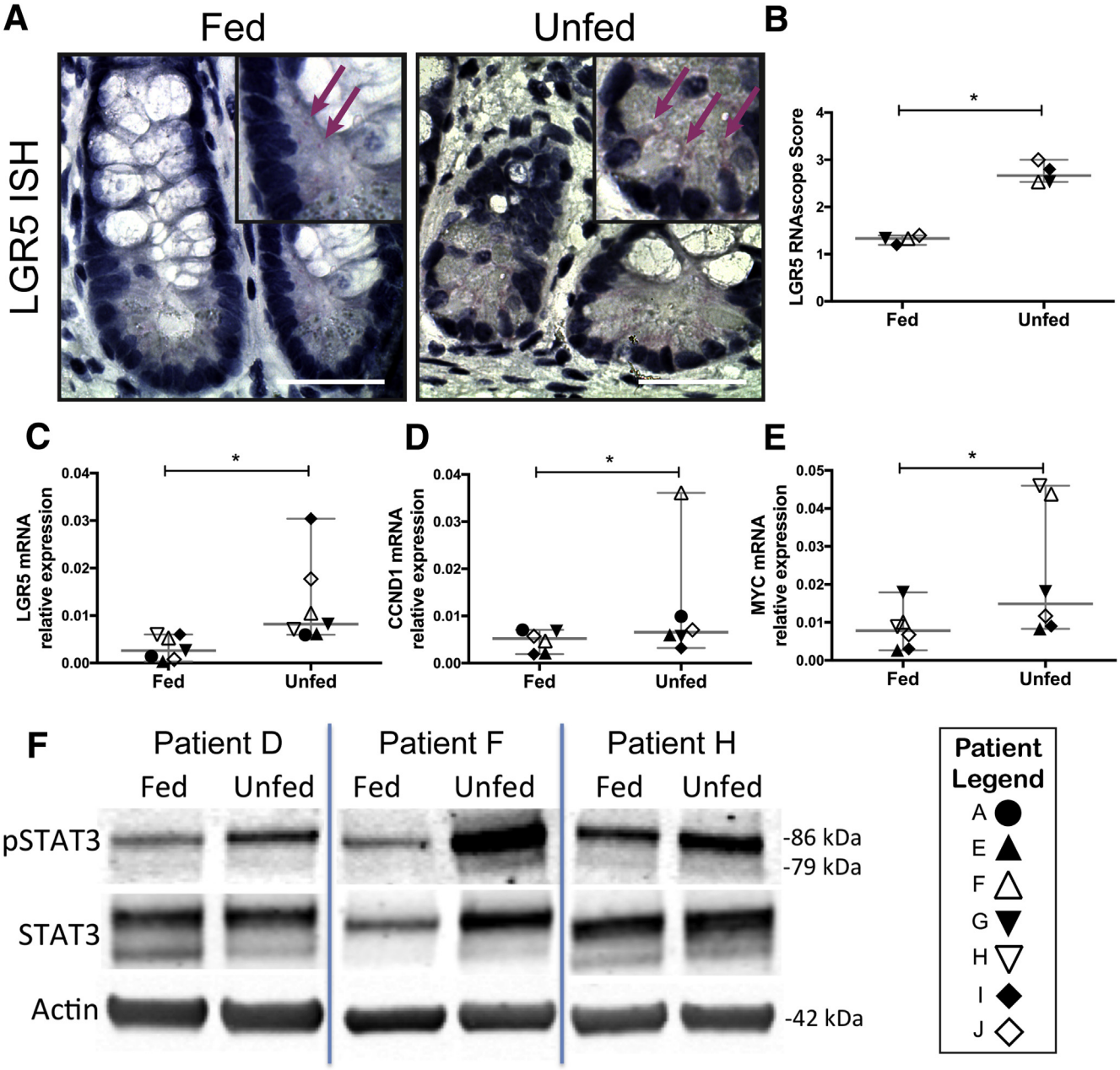

Figure 5. Absence of mechanoluminal stimulation increases *LGR5* mRNA expression and downstream Wnt signaling gene expression. (*A* and *B*) Quantification and in situ hybridization of LGR5 ISCs within the crypts of fed and unfed intestine. *Inset*: High-magnification photographs label LGR5-positive in situ hybridization with *purple arrows*. qPCR comparison of (*C*) *LGR5*, (*D*) *CCND1*, and (*E*) *MYC* mRNA expression between 6 and 7 pairs of matched fed vs unfed intestine with outliers excluded. (*F*) Representative images of Western blot analysis of STAT3 phosphorylation from 3 pairs of matched tissue. Images were obtained on an upright Leica DM5500B immunofluorescence microscope using Leica Suite Advanced Fluorescence (LAS AF) 6000 software, processed with ImageJ software. *Scale bars*: 50 μm. *$P < .05$. *Grey bars* on plots indicate median with 95% confidence interval.

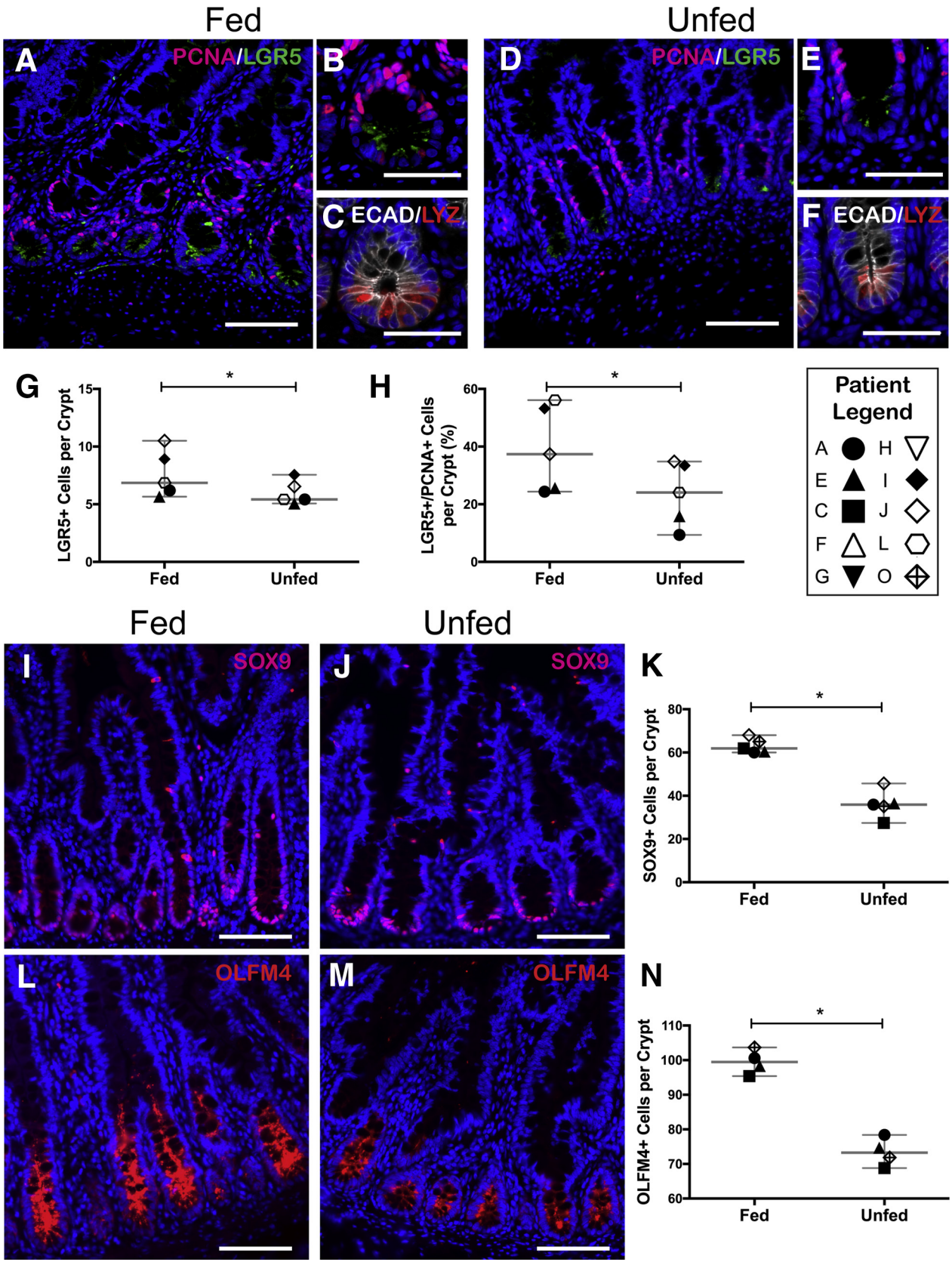
Fed
Unfed
A
PCNA/LGR5
B
C ECAD/LYZ
D
PCNA/LGR5
E
F ECAD/LYZ
G
LGR5+ Cells per Crypt
15
10
5
0
*
Fed
Unfed
H
LGR5+/PCNA+ Cells per Crypt (%)
60
40
20
0
*
Fed
Unfed
Patient Legend
A H
E I
C J
F L
G O
Fed
Unfed
I
SOX9
J
SOX9
K
SOX9+ Cells per Crypt
80
60
40
20
0
*
Fed
Unfed
L
OLFM4
M
OLFM4
N
OLFM4+ Cells per Crypt
110
100
90
80
70
60
*
Fed
Unfed

Expression Omnibus GSE82147, $\log_2$-fold change = 1.68; P = .01) and *ASCL2* (NCBI Gene Expression Omnibus GSE82147, $\log_2$-fold change = 1.49; P = .005) were noted in unfed intestine. Conversely, a down-regulation in *LRIG1* (NCBI Gene Expression Omnibus GSE82147, $\log_2$-fold change = -0.43; P = .05) and *HOPX* (NCBI Gene Expression Omnibus GSE82147, $\log_2$-fold change = -0.80; P = .02) was identified. *SOX9*, *BMI1*, *OLFM4*, *PTEN*, *MTOR*, and *TERT* remained unchanged.

Significantly different genes with $\log_2$-fold change greater than 1.5 involved in immune cell processes, cell proliferation, and apoptosis are shown (Figure 7*C*–*E*). Because all samples were obtained from children with previous NEC or focal intestinal perforation, we sought to determine whether the significant genes associated with immune and inflammatory processes were chronic changes induced by the initial inflammatory insult. Our data were compared with previously reported RNA sequencing–based gene expression profiles from preterm infants with NEC.[36] Comparison of significant pathways in the 2 gene sets showed that inflammation and regulation of inflammation both were over-represented. However, of the 98 genes that were significantly different in both gene expression profiles, only *CXCL5* and *REG1B* had a more than 1.5-fold difference in expression levels in both gene expression profiles.

RNA sequencing identified several growth factors with decreased expression in unfed intestine, such as *WNT2* (NCBI Gene Expression Omnibus GSE82147, $\log_2$-fold change = -2.13; P < .001) and *FGF5* (NCBI Gene Expression Omnibus GSE82147, $\log_2$-fold change = -2.09; P < .001). Of interest, several genes involved in cell proliferation also were involved in immune processes and inflammation. *IL1B*, *IL22*, and *Reg1B* are associated with intestinal inflammation and increased epithelial proliferation.[41,43–46] qPCR confirmed significantly decreased expression of *IL22* (Figure 7*F*) (n = 7; P = .04) and *REG1B* (Figure 7*G*) (n = 6; P = .03) in unfed intestine, but not *IL1B* (Figure 7*H*) (n = 7; P = .0.31).

Discussion

In pediatric human small intestine, we showed that extended absence of mechanoluminal flow in diverted small intestine leads to decreased epithelial cell and ISC proliferation within the crypt, up-regulation of metabolism and transport genes, and down-regulation of inflammatory, immune, and proliferative genes. These effects occur despite adequate caloric intake and provide insight into the importance of mechanoluminal stimulation for normal intestinal adaptation and maintenance of the intestinal epithelium and ISCs. Surgical treatment of acute and chronic intestinal insults often results in diversion of enteral flow. Diversion can vary in location within the gastrointestinal tract and can be variable in time, from short-term withdrawal of enteral feeding, affecting the entire gastrointestinal tract, or partial diversion from an ostomy, resulting in distal deprivation of mechanoluminal flow. Small case series and individual reports have shown improved weight gain and weaning from parenteral nutrition in SBS infants who received enteral nutrition in the distal mucous fistula.[47] However, refeeding of the distal diverted intestine is not widely practiced and the timing and method of enteral feeding in surgical patients remains a contested issue because of conflicting evidence and regional variations in accepted protocols.

Our study suggests that in human beings, mechanoluminal stimulation is required to prevent intestinal atrophy and maintain intestinal homeostasis independent of systemic caloric repletion. In Drosophila, enteral feeding increases gut size and cell number, which is absent during fasting.[48] Starvation is associated with a decrease in villus size, crypt size, and mitotic activity in rats.[22] Calorically restricted mice show decreased mass, villus height, and number of enterocytes within the small intestine.[20] Although infants in our study received adequate caloric intake to promote appropriate weight gain, distal diverted intestine still showed cytoarchitectural characteristics representative of acute animal models of caloric restriction or starvation, including decreased epithelial cell proliferation, villus height, and crypt depth in unfed intestine (Figure 2).

It is unclear if and how mechanoluminal deprivation affected intestinal diameter, length, and mesenchymal components. Neither initial resection specimens representative of a patient's baseline nor full circumferential sections from proximal and distal limbs after diversion were available for comparison of these parameters. However, thinner muscularis mucosae and differences in genes encoding mesenchymal components such as type II collagen were found in unfed intestine on RNA sequencing analysis. The intestinal stroma recently has been identified to provide an intestinal stem cell niche in the absence of epithelial Wnts, suggesting that the stroma can fully support murine intestinal homeostasis.[49] Mechanical and biochemical signaling from the underlying mesenchyme also is believed to play a crucial role in dynamically altering signaling gradients that promote the formation of villi and restrict the ISC population to the base of the crypts.[50] In a porcine model, muscle hypertrophy as a result of massive small-bowel resection potentially helps improve weight gain by slowing

Figure 6. (***See previous page***). **Global decrease of LGR5+, SOX9+, and OLFM4+ intestinal stem cell populations occurs in the absence of mechanoluminal flow.** (*A–H*) Quantification and immunofluorescence staining of LGR5+ rapidly cycling intestinal stem cells per crypt with proliferating cell nuclear antigen counterstain in fed vs unfed intestine. (*C* and *F*) LYZ+ Paneth cells with E-cadherin (Ecad) counterstain of same crypt shown in panels *A* and *D*, respectively, for comparison. (*I–N*) Quantification and immunofluorescence staining of SOX9 and OLFM4 intestinal stem cells per crypt in fed vs unfed intestine. Images were obtained on an upright Leica DM5500B immunofluorescence microscope using Leica Suite Advanced Fluorescence (LAS AF) 6000 software, processed with ImageJ software. *Scale bars*: (*B*, *C*, *E*, and *F*) 50 μm, and (*A*, *D*, *I*, *J*, *L*, and *M*) 100 μm. *P < .05. *Grey bars* on plots indicate median with 95% confidence interval. PCNA, proliferating cell nuclear antigen.

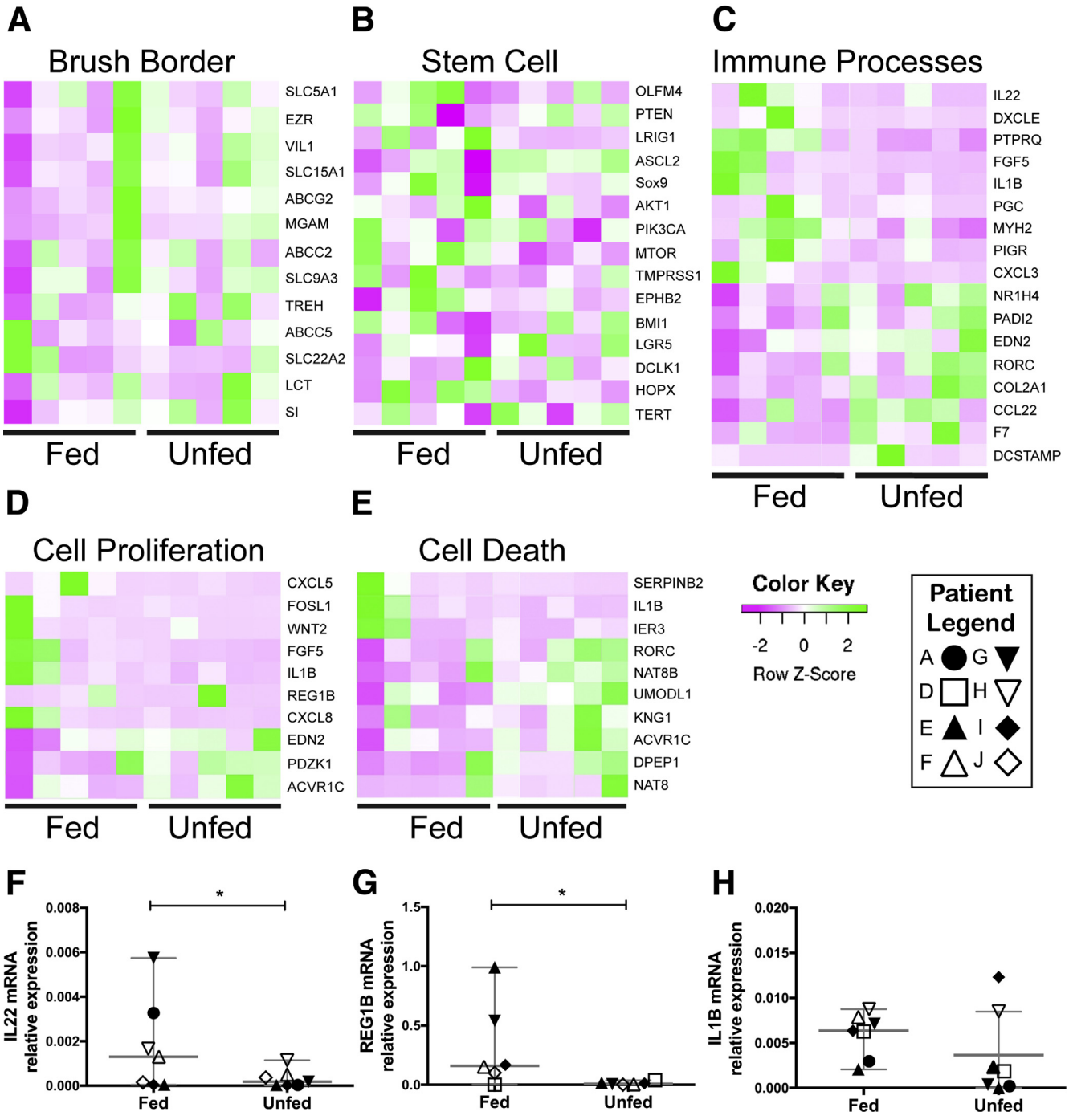

Figure 7. Heatmap representation of biological processes of interest shows differential expression of significant genes between fed and unfed intestine. (*A–E*) Heatmap representation of significantly different genes within biological processes of interest for the 5 pairs analyzed by RNA sequencing. One gene is graphed in each *row* and one intestinal sample is graphed in each *column*. Color represents the expression level with increased expression in green and decreased expression in magenta. (*F–H*) qPCR comparison of pro-proliferative inflammatory genes IL22, REG1B, and IL1B mRNA expression between 6 and 7 pairs of matched fed vs unfed intestine with outliers excluded. *$P < .05$. *Grey bars* on plots indicate median with 95% confidence interval.

gastrointestinal motility and subsequent increase in mucosal absorption.[51,52] Thus, changes in both the intestinal epithelium and the underlying stroma may affect the adaptive capacity of the proximal and distal limbs of the intestine during chronic diversion. Adaptive mechanisms within the stroma that augment epithelial cell proliferation and function may provide useful clinical targets for treating patients with SBS and intestinal failure.

Our study examined a unique intestinal diversion model in which the effect of mechanoluminal stimulation on

intestinal adaptation could be examined without the confounding factor of systemic caloric status, showing an unexpected intestinal stem cell marker expression pattern potentially linked to the relative plasticity and interconversion of various ISCs. Immunofluorescence staining showed a decrease in proliferation that affected differentiated cells in the crypt more than in the villus. Significantly fewer Paneth cells and ISCs were noted in unfed segments, but neither goblet cell nor enteroendocrine cell numbers changed (Figures 2 and 6). Overall, this may represent a shift in differentiation toward a secretory lineage and away from the absorptive lineage. Paneth cells secrete several proliferative signals, including Notch ligand Dll4, epidermal growth factor, transforming growth factor-α, and WNT3 to regulate neighboring ISC activity in the intestinal crypt.[53] Acute caloric restriction in mice has been shown to increase Paneth cell and ISC number while also increasing Paneth cell ability to enhance ISC proliferation and regeneration, leading to intestinal adaptation.[20] In contrast, we found fewer Paneth cells and ISCs in chronically unfed intestine, although, curiously, *LGR5* expression, as shown by qPCR and in situ hybridization, showed increased expression within individual LGR5+ cells. Notably, there appeared to be a decrease in numerous ISC types, including SOX9, OLFM4, and LGR5 stem cells, as shown by immunofluorescence staining (Figure 6). RNA sequencing also showed significant increases in *ASCL2* with a concomitant downregulation of *LRIG1* and *HOPX*.

The adaptability of the intestine during states of injury and acute loss of rapid-cycling ISCs may relate to the relative plasticity of several reserve or dormant stem cell populations that reside within the crypt.[54,55] Cells within the transit-amplifying zone that are in direct contact with Paneth cells can transform into LGR5+ ISCs during damaged states to replete this population.[56] LGR5+ cells can be restored from conversion of HOPX+ cells during acute injury.[57] *BMI1*, *TERT*, *HOPX*, and *LRIG1* have shown significant expression levels within LGR5+ cells, suggesting that all 4 of the +4 markers do not appear to define a single class of ISCs and could play potential roles in interconversion to repopulate lost rapid-cycling ISCs.[55,58] Given the significant decrease in *HOPX* and *LRIG1* shown in our RNA sequencing analysis, these ISC populations could be contributing to restoration of rapid-cycling LGR5+ stem cells.

On RNA sequencing analysis, we also observed a significant increase in expression of *ASCL2*, a direct Wnt pathway target. Wnt signaling is well described as a modulator of intestinal stem cell identity. However, how the crypt to villus signaling gradient is sensed to define epithelial cell types is less understood. *ASCL2* has been reported recently to control ISC stemness by acting as a bimodal switch, forming an autoactivating loop in response to the Wnt signaling gradient, and thereby determining transcriptional activation or repression of downstream Wnt targets.[59,60] Ectopic expression of *ASCL2* induces hyperproliferation of crypts and expansion of SOX9+ and LGR5+ cells within the crypts.[61] In addition, spatial positioning of LGR5+ stem cells within the crypt may affect their availability to enter the cell cycle and influence their propensity to undergo symmetric vs asymmetric division.[62] Given the discordance identified in increased *LGR5* mRNA expression and decreased cell number (Figures 5 and 6), it is plausible that *ASCL2*, another rapid-cycling ISC, regulates *LGR5* downstream effectors in a similar fashion in chronically diverted intestine lacking luminal flow and acts as a master regulator to prime rapid-cycling ISCs in a ready state to contribute to ISC proliferation and epithelial cell differentiation upon the re-introduction of luminal contents.

How ISCs respond to acute changes in intraluminal nutrient sensing and re-feeding remains relatively unknown. In *Drosophila*, feeding activates ISCs, accelerates division rates, and favors symmetric rather than asymmetric division so that the number of stem and total cells increase.[48] In contrast, an increased number of LGR5+ intestinal progenitors and Paneth cells are found in calorically restricted mice when compared with calorically replete mice.[20] Moreover, crypts from these calorically restricted mice show enhanced proliferation and regeneration in the formation of organoids.[20] Richmond et al[63] recently showed that acute nutrient deprivation in mice induces phosphorylation of PTEN in mTert+ ISCs, which release inhibitory signaling of the phosphoinositide 3-kinase/mechanistic target of rapamycin pathway and promotes significant proliferation of the dormant ISC population.[64] We did not observe significant differences in the expression of *TERT*, *BMI1*, *PTEN*, *MTOR*, or *PI3KCA* in the distal limb on RNA sequencing analysis. However, our tissues were obtained from nutritionally replete patients who had undergone diversion for more than 7 weeks, compared with the 48-hour fasting period in the murine model described previously. Although the observations identified by Richmond et al[63] likely may have occurred very early during initial diversion in our patient population, our results reflect mechanisms of intestinal homeostasis and adaptation that occur during chronic absence of mechanoluminal stimulation in a nutritionally replete population. Therefore, enteric feeding and whole-body caloric status may reflect 2 distinct but important activators of ISC proliferation, and controlled animal models investigating chronic mechanoluminal diversion may begin to allow for greater elucidation of luminal signaling mechanisms that could regulate ISC proliferation and intestinal homeostasis. Given our results, we hypothesize that intraluminal cues provided by mechanoluminal stimulation may independently drive intestinal adaptation and regeneration and that absence of mechanoluminal stimulation, particularly in the setting of adequate caloric intake, drives ISC into a less-proliferative, hibernative state.

Numerous biological processes significantly upregulated and down-regulated by the absence of mechanoluminal stimulation indicate that nutrient sensing, biliary secretions, and immune and inflammatory signals all likely play a role in intestinal adaptation. Without mechanoluminal stimulation, unfed intestine increases the expression of genes involved in digestion, transport, and metabolism, perhaps as a feedback loop to optimize and prime nutrient extraction to rapidly accommodate future refeeding.

Interestingly, although protein and carbohydrate pathways are up-regulated, more up-regulated pathways are involved in fatty acid and cholesterol absorption and metabolism. In our RNA sequencing analysis, we identified up-regulation of oxoeicosanoid-receptor 1, a G-protein–coupled receptor, which binds long-chain polyunsaturated fatty acids, in the unfed limb. In embryonic stem cells, unsaturated lipids are crucial for maintenance.[65] Embryonic stem cells express a unique lipid profile high in unsaturated lipids and fatty acids that decrease in differentiated cell states. Upon inhibition of the eicosanoid pathway, pluripotency in embryonic stem cells is maintained as a result of retained levels of unsaturated fatty acids.[66] High-fat diets have been shown to enhance stemness by increasing the number and function of LGR5+ cells through activation of peroxisome proliferator-activated receptor-δ signaling.[67] High-fat diets, and omega-3 fatty acids in particular, also have been shown to enhance adaptation after massive small-bowel resection in rodent models.[68–70] In infants with SBS, fish oil–based intravenous lipid emulsions help ameliorate or reverse cholestasis associated with parenteral nutrition.[70,71] However, no studies have addressed the effect of high-fat enteral diets on adaptation, enteral independence, or weight gain. Because unfed intestine seems primed to absorb and metabolize fats, the effect of high-fat enteral diets should be investigated further.

Although biliary secretions were diverted from unfed intestine, several up-regulated genes also were involved in bile acid metabolism or are associated with hepatic biological processes. For example, *NAT8* and *FMO1* encode enzymes that have been reported previously in fetal liver, but not intestine.[72,73] In vivo, *NAT8* transfection into hepatocytes increases resistance to apoptosis after injury.[73] Little is known about the function of *FMO1* in human intestine, but the adult isoform *FMO2* in nematodes can be activated by dietary restriction and hypoxia to increase nematode life span.[74] Thus, absence of mechanoluminal stimulation induces the expression of genes not previously identified in human intestine. These enzymes may serve a protective role but the function and effect of these novel factors requires further investigation.

The down-regulation on RNA sequencing analysis of genes such as *IL22* involved in inflammation and immune system processes in unfed intestine was somewhat surprising because, clinically, diversion can be associated with inflammation. Except for *REG1B* and *CXCL5*, none of the significantly different genes with fold change greater than 1.5 involved in immune cell processes and inflammation also was significant in active NEC transcriptome analysis.[36] Thus, although NEC resolution seems to be associated with induction of distinct immune process genes in fed intestine, absence of mechanoluminal stimulation in unfed intestine may prevent the same immune process activation. This difference in immune process activation may contribute further to the decreased proliferation in unfed intestine. Interleukin 22 via STAT3 signaling has been shown to promote ISC-mediated regeneration in vivo and increase pancreatic expression of *REG1*, which itself promotes cell-cycle progression and regeneration.[41,75] Several other significant genes also are involved in both immune processes and cell proliferation, such as *CXCL5*, *IL1B*, and *EDN2*. Up-regulated genes also were involved in xenobiotic responses and there is evidence that the microbiome is a major contributor to epithelial integrity and homeostasis.[76,77]

We previously studied whether there was a difference in the pediatric microbiome between fed and unfed intestine. We observed no consistent difference; in fact, the microbiota of the unfed intestine most resembled its paired fed intestine.[78] Thus, mechanoluminal stimulation also may be required for immune recovery, cross-talk with the microbiome, and/or maintenance and proliferation of ISCs after disease insult. Multiple growth factors have been identified that enhance adaptation in animal models, such as growth hormone, insulin-like growth factor-1, epidermal growth factor, glucagon-like peptide 2, and steroids.[10] Of these, growth hormone and glucagon-like peptide 2 have shown promising results in improving nutrient absorption and weight gain in human patients with SBS.[11–13] In our study, RNA sequencing analysis did not show any significant difference in levels of mRNA for growth hormone receptor, epidermal growth factor, insulin-like growth factor-1, epidermal growth factor receptor, or glucagon-like peptide 2 receptor. Growth hormone and glucagon-like peptide 2 were not among the sequenced genes. Genes involved in steroid secretion and response to steroids were significantly down-regulated in unfed intestine. Thus, the factors and pathways affecting adaptation after small-bowel resection may differ from those affected by mechanoluminal stimulation. Alternatively, different factors may peak at variable times and after several weeks of diversion, expression of these previously identified growth factors already may have waned. However, it is possible that the RNA sequencing analysis may not have been powered adequately to detect differences in these humoral factors, or that protein expression and pathway activation may have been significantly different without differences in mRNA expression. As with most studies of complex processes in human tissue, these data are limited by the small sample size, finite tissue specimens, and the inability to define the cellular location of the transcriptional events. To minimize variability and confounding resulting from patient factors, a very narrow set of patients was studied and internally controlled by accessing paired specimens in close anatomic approximation to avoid regional physiologic and genetic differences. Because intestine is undergoing rapid development during infancy and childhood, the mechanisms driving and regulating proliferation and adaptation in adult intestine may be different.

Nonetheless, these data provide new insight into the human intestinal response to chronic absence of luminal stimulation and the signaling that governs small intestine proliferation and adaptation. The broad effects of mechanoluminal deprivation on intestinal structure and function emphasize the importance of enteral nutrition in the treatment of short-bowel syndrome. Overall, nutrition status and enteral flow provide 2 distinct environmental cues for the intestine with important effects on intestinal homeostasis

and adaptation. As we seek to better understand the mechanisms driving intestinal adaptation and regeneration, these data may enable future identification of novel therapeutic targets for treatment of patients with SBS and intestinal failure.

References

1. Vegge A, Thymann T, Lund P, et al. Glucagon-like peptide-2 induces rapid digestive adaptation following intestinal resection in preterm neonates. Am J Physiol Gastrointest Liver Physiol 2013;305:G277–G285.
2. Schall KA, Holoyda KA, Grant CN, et al. Adult zebrafish intestine resection: a novel model of short bowel syndrome, adaptation, and intestinal stem cell regeneration. Am J Physiol Gastrointest Liver Physiol 2015;309:G135–G145.
3. Sangild PT, Ney DM, Sigalet DL, et al. Animal models of gastrointestinal and liver diseases. Animal models of infant short bowel syndrome: translational relevance and challenges. Am J Physiol Gastrointest Liver Physiol 2014;307:G1147–G1168.
4. Helmrath MA, VanderKolk WE, Can G, et al. Intestinal adaptation following massive small bowel resection in the mouse. J Am Coll Surg 1996;183:441–449.
5. Schall KA, Holoyda KA, Isani M, et al. Inhibition of Fgf signaling in short bowel syndrome increases weight loss and epithelial proliferation. Surgery 2017;161:694–703.
6. McDuffie LA, Bucher BT, Erwin CR, et al. Intestinal adaptation following small bowel resection in human infants. J Pediatr Surg 2011;46:1045–1051.
7. Doldi SB. Intestinal adaptation following jejuno-ileal bypass. Clin Nutr 1991;10:138–145.
8. Porus RL. Epithelial hyperplasia following massive small bowel resection in man. Gastroenterology 1965;48:753–757.
9. Warner BW. The pathogenesis of resection-associated intestinal adaptation. Cell Mol Gastroenterol Hepatol 2016;2:429–438.
10. McMellen ME, Wakeman D, Longshore SW, et al. Growth factors: possible roles for clinical management of the short bowel syndrome. Semin Pediatr Surg 2010;19:35–43.
11. Sigalet DL, Brindle M, Boctor D, et al. A safety and dosing study of glucagon-like peptide 2 in children with intestinal failure. JPEN J Parenter Enteral Nutr 2015 Oct 15. pii: 0148607115609566. [Epub ahead of print].
12. Schwartz LK, O'Keefe SJ, Fujioka K, et al. Long-term teduglutide for the treatment of patients with intestinal failure associated with short bowel syndrome. Clin Transl Gastroenterol 2016;7:e142.
13. Guo MX, Li YS, Fan L, et al. Growth hormone for intestinal adaptation in patients with short bowel syndrome: systematic review and meta-analysis of randomized controlled trials. Curr Ther Res Clin Exp 2011;72:109–119.
14. Williamson RC. Intestinal adaptation (first of two parts). Structural, functional and cytokinetic changes. N Engl J Med 1978;298:1393–1402.
15. Sukhotnik I, Berkowitz D, Dorfman T, et al. The role of the BMP signaling cascade in regulation of stem cell activity following massive small bowel resection in a rat. Pediatr Surg Int 2016;32:169–174.
16. Sukhotnik I, Lulu SB, Pollak Y, et al. TGF-beta affects enterocyte turnover in correlation with TGF-beta receptor expression after massive small bowel resection. J Pediatr Gastroenterol Nutr 2012;55:721–727.
17. Gosselin KB, Duggan C. Enteral nutrition in the management of pediatric intestinal failure. J Pediatr 2014;165:1085–1090.
18. Andorsky DJ, Lund DP, Lillehei CW, et al. Nutritional and other postoperative management of neonates with short bowel syndrome correlates with clinical outcomes. J Pediatr 2001;139:27–33.
19. Sondheimer JM, Cadnapaphornchai M, Sontag M, et al. Predicting the duration of dependence on parenteral nutrition after neonatal intestinal resection. J Pediatr 1998;132:80–84.
20. Yilmaz OH, Katajisto P, Lamming DW, et al. mTORC1 in the Paneth cell niche couples intestinal stem-cell function to calorie intake. Nature 2012;486:490–495.
21. Ralls MW, Demehri FR, Feng Y, et al. Enteral nutrient deprivation in patients leads to a loss of intestinal epithelial barrier function. Surgery 2015;157:732–742.
22. Altmann GG. Influence of starvation and refeeding on mucosal size and epithelial renewal in the rat small intestine. Am J Anat 1972;133:391–400.
23. Dame MK, Jiang Y, Appelman HD, et al. Human colonic crypts in culture: segregation of immunochemical markers in normal versus adenoma-derived. Lab Invest 2014;94:222–234.
24. Busby MA, Stewart C, Miller CA, et al. Scotty: a web tool for designing RNA-Seq experiments to measure differential gene expression. Bioinformatics 2013;29:656–657.
25. Bioinformatics B. FastQC a quality control tool for high throughput sequence data 2016. Available from: http://www.bioinformatics.babraham.ac.uk/projects/fastqc/.
26. Bolger AM, Lohse M, Usadel B. Trimmomatic: a flexible trimmer for Illumina sequence data. Bioinformatics 2014;30:2114–2120.
27. Dobin A, Davis CA, Schlesinger F, et al. STAR: ultrafast universal RNA-seq aligner. Bioinformatics 2013;29:15–21.
28. Harrow J, Frankish A, Gonzalez JM, et al. GENCODE: the reference human genome annotation for The ENCODE Project. Genome Res 2012;22:1760–1774.
29. Anders S, Pyl PT, Huber W. HTSeq–a Python framework to work with high-throughput sequencing data. Bioinformatics 2015;31:166–169.
30. Robinson MD, McCarthy DJ, Smyth GK. edgeR: a Bioconductor package for differential expression analysis of digital gene expression data. Bioinformatics 2010;26:139–140.
31. Zhang J, Carey V, Gentleman R. An extensible application for assembling annotation for genomic data. Bioinformatics 2003;19:155–156.
32. Risso D, Schwartz K, Sherlock G, et al. GC-content normalization for RNA-Seq data. BMC Bioinformatics 2011;12:480.

33. Risso D, Ngai J, Speed TP, et al. Normalization of RNA-seq data using factor analysis of control genes or samples. Nat Biotechnol 2014;32:896–902.
34. Falcon S, Gentleman R. Using GOstats to test gene lists for GO term association. Bioinformatics 2007;23:257–258.
35. Maere S, Heymans K, Kuiper M. BiNGO: a Cytoscape plugin to assess overrepresentation of gene ontology categories in biological networks. Bioinformatics 2005; 21:3448–3449.
36. Tremblay É Thibault MP, Ferretti E, et al. Gene expression profiling in necrotizing enterocolitis reveals pathways common to those reported in Crohn's disease. BMC Med Genomics 2015;9:6.
37. Motulsky HJ, Brown RE. Detecting outliers when fitting data with nonlinear regression - a new method based on robust nonlinear regression and the false discovery rate. BMC Bioinformatics 2006;7:123.
38. Barker N. Adult intestinal stem cells: critical drivers of epithelial homeostasis and regeneration. Nat Rev Mol Cell Biol 2013;15:19–33.
39. Barker N, Tan S, Clevers H. Lgr proteins in epithelial stem cell biology. Development 2013;140:2484–2494.
40. Matthews JR, Sansom OJ, Clarke AR. Absolute requirement for STAT3 function in small-intestine crypt stem cell survival. Cell Death Differ 2011;18:1934–1943.
41. Lindemans CA, Calafiore M, Mertelsmann AM, et al. Interleukin-22 promotes intestinal-stem-cell-mediated epithelial regeneration. Nature 2015;528:560–564.
42. Yu H, Lee H, Herrmann A, et al. Revisiting STAT3 signalling in cancer: new and unexpected biological functions. Nat Rev Cancer 2014;14:736–746.
43. Murano T, Okamoto R, Ito G, et al. Hes1 promotes the IL-22-mediated antimicrobial response by enhancing STAT3-dependent transcription in human intestinal epithelial cells. Biochem Biophys Res Commun 2014; 443:840–846.
44. Leal RF, Planell N, Kajekar R, et al. Identification of inflammatory mediators in patients with Crohn's disease unresponsive to anti-TNFα therapy. Gut 2015; 64:233–242.
45. van Beelen Granlund A, Østvik AE, Brenna Ø, et al. REG gene expression in inflamed and healthy colon mucosa explored by in situ hybridisation. Cell Tissue Res 2013; 352:639–646.
46. Wang L, Liu Z, Li Y, et al. Pro-inflammatory cytokine interleukin-1beta promotes the development of intestinal stem cells. Inflamm Res 2012;61:1085–1092.
47. Richardson L, Banerjee S, Rabe H. What is the evidence on the practice of mucous fistula refeeding in neonates with short bowel syndrome? J Pediatr Gastroenterol Nutr 2006;43:267–270.
48. O'Brien LE, Soliman SS, Li X, et al. Altered modes of stem cell division drive adaptive intestinal growth. Cell 2011;147:603–614.
49. Kabiri Z, Greicius G, Madan B, et al. Stroma provides an intestinal stem cell niche in the absence of epithelial Wnts. Development 2014;141:2206–2215.
50. Shyer AE, Huycke TR, Lee C, et al. Bending gradients: how the intestinal stem cell gets its home. Cell 2015; 161:569–580.
51. Pereira-Fantini PM, Thomas SL, Taylor RG, et al. Colostrum supplementation restores insulin-like growth factor-1 levels and alters muscle morphology following massive small bowel resection. JPEN J Parenter Enteral Nutr 2008;32:266–275.
52. Nagy ES, Paris MC, Taylor RG, et al. Colostrum protein concentrate enhances intestinal adaptation after massive small bowel resection in juvenile pigs. J Pediatr Gastroenterol Nutr 2004;39:487–492.
53. Sato T, van Es JH, Snippert HJ, et al. Paneth cells constitute the niche for Lgr5 stem cells in intestinal crypts. Nature 2011;469:415–418.
54. Barker N, van Oudenaarden A, Clevers H. Identifying the stem cell of the intestinal crypt: strategies and pitfalls. Cell Stem Cell 2012;11:452–460.
55. Tetteh PW, Basak O, Farin HF, et al. Replacement of lost Lgr5-positive stem cells through plasticity of their enterocyte-lineage daughters. Cell Stem Cell 2016; 18:203–213.
56. Tian H, Biehs B, Warming S, et al. A reserve stem cell population in small intestine renders Lgr5-positive cells dispensable. Nature 2011;478:255–259.
57. Takeda N, Jain R, LeBoeuf MR, et al. Interconversion between intestinal stem cell populations in distinct niches. Science 2011;334:1420–1424.
58. Powell AE, Wang Y, Li Y, et al. The pan-ErbB negative regulator Lrig1 is an intestinal stem cell marker that functions as a tumor suppressor. Cell 2012; 149:146–158.
59. Schuijers J, Junker JP, Mokry M, et al. Ascl2 acts as an R-spondin/Wnt-responsive switch to control stemness in intestinal crypts. Cell Stem Cell 2015;16:158–170.
60. Yan KS, Kuo CJ. Ascl2 reinforces intestinal stem cell identity. Cell Stem Cell 2015;16:105–106.
61. van der Flier LG, van Gijn ME, Hatzis P, et al. Transcription factor achaete scute-like 2 controls intestinal stem cell fate. Cell 2009;136:903–912.
62. Moossavi S. Heterogeneity of the level of activity of lgr5+ intestinal stem cells. Int J Mol Cell Med 2014;3:216–224.
63. Richmond CA, Shah MS, Deary LT, et al. Dormant intestinal stem cells are regulated by PTEN and nutritional status. Cell Rep 2015;13:2403–2411.
64. Sailaja BS, He XC, Li L. Stem cells matter in response to fasting. Cell Rep 2015;13:2325–2326.
65. Ochocki JD, Simon MC. Nutrient-sensing pathways and metabolic regulation in stem cells. J Cell Biol 2013; 203:23–33.
66. Yanes O, Clark J, Wong DM, et al. Metabolic oxidation regulates embryonic stem cell differentiation. Nat Chem Biol 2010;6:411–417.
67. Beyaz S, Mana MD, Roper J, et al. High-fat diet enhances stemness and tumorigenicity of intestinal progenitors. Nature 2016;531:53–58.
68. Choi PM, Sun RC, Guo J, et al. High-fat diet enhances villus growth during the adaptation response to massive proximal small bowel resection. J Gastrointest Surg 2014;18:286–294.
69. Choi PM, Sun RC, Sommovilla J, et al. The role of enteral fat as a modulator of body composition after small bowel resection. Surgery 2014;156:412–418.

70. Kollman KA, Lien EL, Vanderhoof JA. Dietary lipids influence intestinal adaptation after massive bowel resection. J Pediatr Gastroenterol Nutr 1999;28:41–45.
71. Chung PH, Wong KK, Wong RM, et al. Clinical experience in managing pediatric patients with ultra-short bowel syndrome using omega-3 fatty acid. Eur J Pediatr Surg 2010;20:139–142.
72. Chen Y, Zane NR, Thakker DR, et al. Quantification of flavin-containing monooxygenases 1, 3 and 5 in human liver microsomes by UPLC-MRM-based targeted quantitative proteomics and its application to the study of ontogeny. Drug Metab Dispos 2016;44:975–983.
73. Fu J, Zhang H, Zhuang Y, et al. The role of N-acetyltransferase 8 in mesenchymal stem cell-based therapy for liver ischemia/reperfusion injury in rats. PLoS One 2014;9:e103355.
74. Leiser SF, Miller H, Rossner R, et al. Cell nonautonomous activation of flavin-containing monooxygenase promotes longevity and health span. Science 2015;350:1375–1378.
75. Hill T, Krougly O, Nikoopour E, et al. The involvement of interleukin-22 in the expression of pancreatic beta cell regenerative Reg genes. Cell Regen (Lond) 2013;2:2.
76. Demehri FR, Barrett M, Ralls MW, et al. Intestinal epithelial cell apoptosis and loss of barrier function in the setting of altered microbiota with enteral nutrient deprivation. Front Cell Infect Microbiol 2013;3:105.
77. Maslowski KM, Mackay CR. Diet, gut microbiota and immune responses. Nat Immunol 2011;12:5–9.
78. Wieck MM, Debelius JW, Spurrier RG, et al. The pediatric intestinal mucosal microbiome remains altered after clinical resolution of inflammatory and ischemic disease. Surgery 2016;160:350–358.

Received June 8, 2016. Accepted December 20, 2016.

Correspondence
Address correspondence to: Tracy C. Grikscheit, MD, The Saban Research Institute, Children's Hospital Los Angeles, 4650 W Sunset Boulevard, MS#100, Los Angeles, California 90027. e-mail: tgrikscheit@chla.usc.edu; fax: (323) 361-1546.

Acknowledgments
The authors thank the Department of Pathology, Children's Hospital Los Angeles, G. Esteban Fernandez, PhD, and the Imaging core, The Saban Research Institute at Children's Hospital, Los Angeles. The authors thank Jason Spence and his laboratory for their kind assistance with LGR5 staining.

Minna M. Wieck, Christopher R. Schlieve, Christa N. Grant, and Tracy C. Grikscheit were responsible for the study concept and design; Minna M. Wieck, Christopher R. Schlieve, Kathryn L. Fowler, Mubina Isani, Christa N. Grant, Matthew Thornton, Ashley E. Hilton, Xiaogang Hou, and Brendan Grubbs acquired data; Minna M. Wieck, Christopher R. Schlieve, Kathryn L. Fowler, Matthew Thornton, Mark R. Frey, and Tracy C. Grikscheit analyzed and interpreted data; Minna M. Wieck, Christopher R. Schlieve, and Christa N. Grant drafted the manuscript; and Minna M. Wieck, Christopher R. Schlieve, Matthew Thornton, Mark R. Frey, and Tracy C. Grikscheit critically revised the manuscript.

Conflicts of interest
The authors disclose no conflicts.

Funding
Supported by National Institutes of Health award R01DK095004 (T.C.G.).

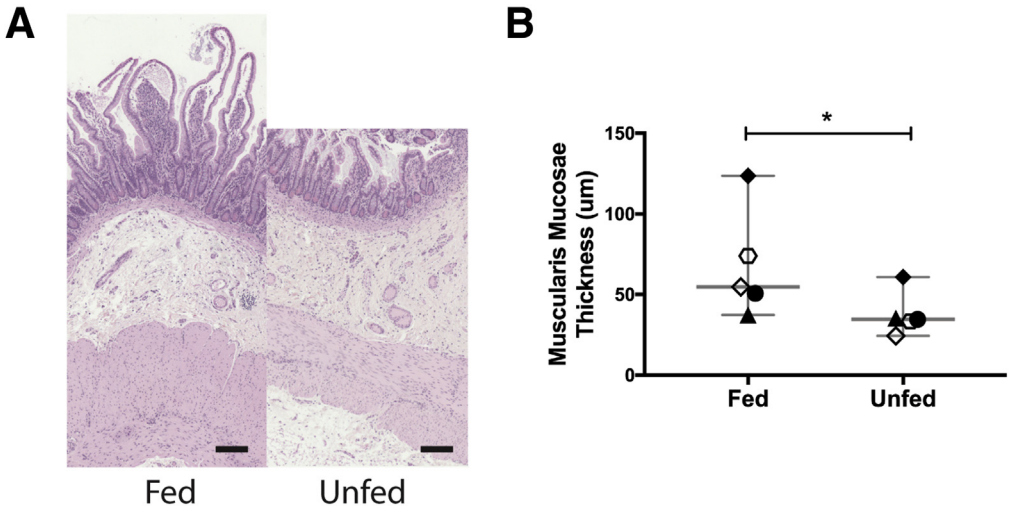

Supplementary Figure 1. (*A*) **H&E analysis of full-thickness intestinal tissue sections verified that the stroma between fed and unfed intestine remained otherwise nonreactive with no marked changes in cytoarchitecture outside of** (*B*) **a significant decrease in the thickness of the muscularis mucosae.** *Scale bars*: 200 μm. *$P < .05$.